WestVirginiaUniversity
THE RESEARCH REPOSITORY @ WVU

Graduate Theses, Dissertations, and Problem Reports

1992

Secondary dust generation in rotary coal cutting.

Danqing Xu

Follow this and additional works at: https://researchrepository.wvu.edu/etd

INFORMATION TO USERS

This manuscript has been reproduced from the microfilm master. UMI films the text directly from the original or copy submitted. Thus, some thesis and dissertation copies are in typewriter face, while others may be from any type of computer printer.

The quality of this reproduction is dependent upon the quality of the copy submitted. Broken or indistinct print, colored or poor quality illustrations and photographs, print bleedthrough, substandard margins, and improper alignment can adversely affect reproduction.

In the unlikely event that the author did not send UMI a complete manuscript and there are missing pages, these will be noted. Also, if unauthorized copyright material had to be removed, a note will indicate the deletion.

Oversize materials (e.g., maps, drawings, charts) are reproduced by sectioning the original, beginning at the upper left-hand corner and continuing from left to right in equal sections with small overlaps. Each original is also photographed in one exposure and is included in reduced form at the back of the book.

Photographs included in the original manuscript have been reproduced xerographically in this copy. Higher quality 6" x 9" black and white photographic prints are available for any photographs or illustrations appearing in this copy for an additional charge. Contact UMI directly to order.

Order Number 9322947

Secondary dust generation in rotary coal cutting

Xu, Danqing, Ph.D.

West Virginia University, 1992

U·M·I
300 N. Zeeb Rd.
Ann Arbor, MI 48106

SECONDARY DUST GENERATION IN ROTARY COAL CUTTING

by

Danqing Xu

A Dissertation

Submitted to the Faculty of

Department of Mining Engineering

College of Mineral and Energy Resources

West Virginia University

In Partial Fulfillment of the Requirements

for the Degree of

Doctor of Philosophy

in

Mining Engineering

Morgantown, West Virginia

August 1992

ABSTRACT

In a rotary coal cutting system, the mined coal has to be transported through the cutting path. This transportation of mined coal through the cutting zone of a rotary cutting head is comparable to a rotary grinder. In the "grinder", the mined coal particles are subjected to secondary comminution, known as regrinding. A significant amount of coal dust could be generated during regrinding. This study was undertaken to investigate the mechanisms of regrinding and dust generation, to quantify the amount of dust generated during regrinding and evaluate the effects of influencing parameters on dust generation.

Three comminution mechanisms of particles in the regrinding process, namely slow compression, impact, and attrition, were recognized. Compression and dust generation were studied utilizing an electro-hydraulic servo control testing machine, with a controlled displacement rate of 0.00025 cm/s. A dynamic finite element model was employed to study impact failure. Dust generation due to impact failure was observed using a high speed video camera system. It was found that compression and impact generate dust because they create a crushed zone under the contact area. Dust generation by attrition was also investigated and it was found that attrition of coal particles generates a significant amount of dust.

An Automated Rotary Coal Cutting Simulator was utilized to simulate the regrinding process. Laboratory simulation studies showed that the amount of feed particles subjected to compression and impact breakage was only 5%~11% and it decreased as feed particle size decreased. But the amount of dust generated during regrinding was significant and it increased as feed particle size decreased. This indicates that attrition of coal particles is the primary mechanism of the secondary dust generation.

An orthogonal fractional factorial experiment was conducted to estimate the effects of the major parameters on dust generation during regrinding. Experimental results showed that the amount of dust generated increased with increasing depth of sump, cutting velocity, and grindability index of coal materials. Dust generation during regrinding can be reduced by increasing the particle size in the product of the primary cutting, reducing the depth of sump and cutting velocity.

ACKNOWLEDGEMENTS

TABLE OF CONTENTS

Content   **Page**

LIST OF TABLES

LIST OF FIGURES

Chapter 1
INTRODUCTION

Dust control has recently received more attention in the mining industry because of its potential for physiological harm and explosion hazard. The most serious occupational disease in the mining industry, black lung, is caused by the accumulation of insoluble respirable coal dust in the lungs. The incidence of black lung depends on the physiological property of dust, dust concentration, and the duration of exposure. But the dust concentration is the most important parameter for the assessment of the incidence of black lung. To prevent coal workers from having black lung, MSHA has established a very stringent dust concentration standard for coal mining operations (2.0 mg/m^3 with silica content equal to or less than 0.1 mg/m^3). A key to control dust concentration, at or below the standard established by Federal legislation, is to utilize various dust control techniques in each operation process.

Research efforts involved in the last decade included dust prevention, suppression, collection, and dust sampling. Studies over the last decade showed that controlling the formation of respirable dust during coal extraction was one of the most effective means of reducing worker's exposure (Daniel 1984). Daniel

stated "Major causes of dust formation appear to be localized crushing at the bit-coal interface, creation of new surfaces remote from the bit, and secondary comminution (regrinding) caused by the action of the mining machine drum." In other words, coal cutting includes primary fragmentation and regrinding. Primary fragmentation cuts coal from the intact coal seam and generates primary coal dust because of the crushing at the bit-coal interface and the formation of new surfaces. Regrinding takes place because all mined coal and part of the remainder coal from previous cutting cycles have to be transported through part of or the entire length of the cutting path of a rotary cutting system. This transportation of already mined coal through the cutting zone of a rotary cutting head is comparable to a rotary grinder (Repoke 1984). The coal particles will be comminuted in the "grinder." It further reduces the size of coal particles, increases the total surface area of coal particles, frees materials from its matrices and generates secondary coal dust.

In the primary fragmentation, the crushed zone is the major source of airborne dust (Repoke 1984, Khair 1984). Crushing occurs when a bit indents and penetrates a coal seam. The indentation and penetration of the bit create three damage zones, namely, crushed zone, chipped zone and fractured zone. Crushed zone is right around the bit tip and its size and shape primarily depend on the size and geometry of the carbide tip and bit body. Many other parameters, such as spacing, the depth of cut, cutting velocity, bit-mounting configuration, the

2

properties of coal material and in-situ stress conditions, also significantly affect the characteristics of the damage zones. To reduce the amount of dust generated during the primary fragmentation, a number of researchers have suggested modification of the cutting head and the cutting bits, and the operating parameters.

But the process of regrinding and the generation of the secondary coal dust have not been investigated. This study was undertaken to analyze the mechanism of regrinding and resulting dust generation, develop a mathematical formulation of the regrinding process, quantify the amount of dust generated by regrinding per unit weight of coal cut and evaluate the effects of operating parameters and coal properties on dust generation due to regrinding. The intents of this research were to answer the following questions:

1) How is dust generated in the secondary comminution?

2) How significant is the secondary dust generation for airborne dust levels?

3) What are the primary factors affecting the secondary dust generation?

4) How to control the secondary dust generation?

Chapter 2
LITERATURE REVIEW

The regrinding process is actually a size reduction process. The principle of regrinding is similar to that of other size reduction means, such as crushing and grinding. Size reduction process is complicated and the literature concerning size reduction is very extensive, including the mechanism of size reduction, the relationship between size reduction and energy consumption, and the mathematical simulation. The following sections present a brief review of studies concerning each area of size reduction.

MECHANISM OF SIZE REDUCTION

Although size reduction machines in current use, such as jaw crusher and impact mill, incorporate an assemblage of particles, multiple breakages and different breakage patterns, it is important to understand the principles of single particle breakage and distinguish breakage patterns. Prasher (1987) presented four methods of force application to a particle associated with different breakage patterns in size reduction process:

1) Compression - particle disintegration between two rigid forces,

2) Impact - particle concussion by a single rigid force,

3) Shear - the wrenching apart of a particle by the action of a rigid force

   or the swirling of a fluid, and

4) Attrition - the scraping of one surface on another.

Studies of Compression

Utilizing disc, cubic, and spherical specimens, Jaeger (1967) examined,

theoretically and experimentally, the failure of specimens under a different number

and direction of compressive forces (crushing forces). He concluded that failure

was invariably in almost straight lines joining the loading points. Failure therefore

followed very closely the lines of maximum tensile stress even if it was not initiated

on these lines. A full review of the studies of the three-dimensional stress pattern

and failure pattern of a particle under the influence of applied compressive forces

was presented by Prasher (1987). He stated that the stress pattern produced in the

particle was dependent on the number and direction of forces, material properties,

rate of deformation and particle size and shape. Under two or more compressive

forces, cracks developed from any one contact point in the direction of another

force contact point and formed a wedge or cone shape crushed zone under each

force contact point, as illustrated in Figure 2.1. The breakage probability within an

assemblage of spheres increased with the number of contact points per particle up

to a limited number of the order of ten. If more contact points were developed, the breakage probability decreased and greater was the tendency for cracks to run near the periphery of the particle.
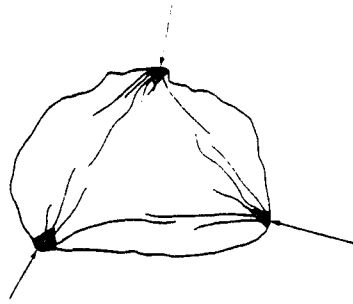
Figure 2.1 Typical crushing failure pattern (after Prasher, 1987)

Pressure distribution on a contact area and failure under contact points have received great attention. If a sphere is compressed by a weighted horizontal hard flat plate, the sphere will deform, giving a circular contact area. Zukas (1982) stated that the distribution of contact force on the contact area was a semi-sphere. Angel (1976) demonstrated the process of contact of spheres and final pressure distribution on the contact area as shown in Figure 2.2. The maximum pressure was 1.5 times the average pressure. Hamilton and Goodman (1966) found that the highest tensile stress occurred round the edge of the contact area, giving rise to a ring crack. Within this ring, in a cone-shape volume, lesser tensile stresses occurred. Prasher (1987) thought that since highest contact pressure was 1.5 times

6

the average pressure, the shear stress could be up to 75% of the average pressure. This indicated that the intensity of the stresses just below the contact area was much greater than that in the rest of the particle. Hence, a more intense size reduction would be predicted for the material in the cone below the contact area.
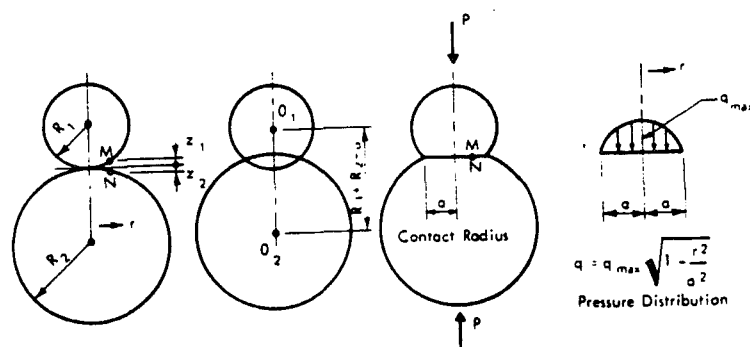
Figure 2.2. Contact process and pressure distribution on contact area
(after Angel, 1976)

The effect of applied forces on the parts other than the contact area was also well studied. Prasher (1987) presented Schonert's studies of the strain pattern in a particle under the influence of two compressive forces in great detail. Two sets of strain gages, four gages per sets, were equipped on a 50 mm sphere of steel, as shown in Figure 2.3. One set was secured on a meridian, in the yz plane, and lying in the direction of the meridian, to give the longitudinal strain. The other set

7

was placed in a meridian, in the xz plane, and lying in the latitudinal direction to give latitudinal strain. When a load of 2500 kg was applied, the resulting strain patterns are shown in Figure 2.4. Strain pattern for elastic material is rather different from that for the plastic. According to the strain distribution, crack patterns were predicted. For elastic material, as shown in Figure 2.5, 1) ring and cone cracks would develop around the contact circle because of the high longitudinal tensile stress, 2) cracks would run around curved surfaces like an onion peel following surfaces of constant strain, 3) no meridional cracks would appear because of the low latitudinal tensile stress. For plastic material, high latitudinal tensile strains occurred around the contact area because beneath it a cone-shaped volume was driven into the sphere by the applied forces, pushing the surrounding material sideways and upwards along logarithmic spirals. The outer shell was thus strained as if the sphere were under internal pressure. Associated with this lateral tensile strain would be lateral tensile stress, and hence cracks parallel to meridional planes would be forecast, dividing the sphere into fragments as shown in Figure 2.6.
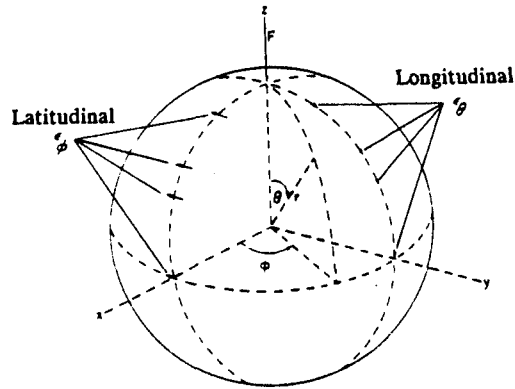
Figure 2.3. Position of strain gages on an experimental sphere
(after Prasher, 1987)
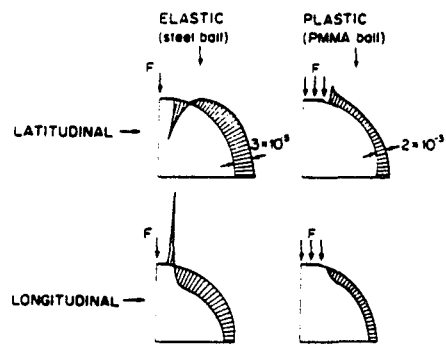
Figure 2.4. Strain pattern resulted from a radially applied force on elastic
and plastic material, shaded areas indicate the degree of strain,
tensile strain is outside and compressive strain is inside the
quadrants, (after Prasher, 1987)

9
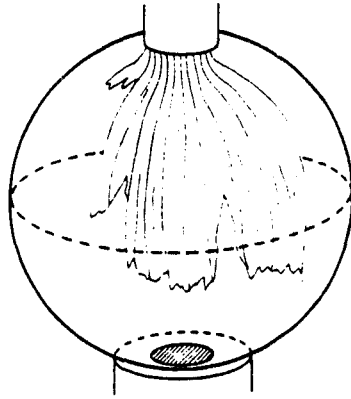
Figure 2.5. Crack pattern within an elastic sphere under an applied radial compressive force (after prasher, 1987)
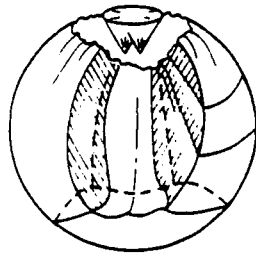
Figure 2.6. Crack pattern within a plastic sphere under a radially applied force (after Prasher, 1987)

Studies of Impact Failure

The difficulty in the study of impact failure is that it is transient and it is hard to obtain a stress patterns through experiments. One of the methods to study impact failure is to find out the impact force on a body and then analyze the internal stress distribution in the body under the influence of this force. A theoretical solution of the impact force, when two solid spherical bodies undergo central elastic impact, was given by Johnson (1972), as expressed in Equation (2.1):

$$P = kx^{\frac{2}{3}} \qquad (2.1)$$

where P is impact force, x is the distance of approaching between the two bodies, and k is a constant, depending on the size and properties of the bodies. For the particular case in which a spherical body impacts a semi-infinite body, the maximum impact force can be determined by Equation (2.2) (Johnson, 1972):

$$P_{max} = \frac{4R_2^{\frac{1}{3}}(\frac{15}{16}\pi m_2 v_0^2)^{\frac{3}{5}}}{3\pi(\frac{1-v_1^2}{\pi E_1} + \frac{1-v_2^2}{\pi E_2})^{\frac{2}{5}}} \qquad (2.2)$$

where R_2, m_2, v_0, E_2, and v_2 are the radius, mass, initial impact velocity, Young's modulus and Poisson's ratio of the spherical body, respectively. E_1, v_1 are Young's

modulus and Poisson's ratio of the semi-infinite body, respectively. For an irregularly shaped particle, however, the problem will become so complicated that it could not be solved.

Particle failure may be caused by excessive compressive stress, shear stress near contact area, or tensile stress in particle. Rineheart (1960) pointed out that stress wave could play a dominant role in impact comminution processes. Rock can effectively transmit high stresses to regions remote from the source because of its high compressive strength. On reflection the stresses may be transformed into destructive tensile stress in rock which is weak in tension.

In studying the principles of impact mills, Lowrison (1974) stated that particles broke because the kinetic energy of a mill was transformed into internal strain energy of particles. When enough kinetic energy is transformed, the internal strain energy in a particle can cause the particle to shatter. If the energy transformation is perfect, the relationship between kinetic energy and strain energy for a single particle would be:

$$\frac{mv^2}{2} = \frac{\sigma^2}{2E}Q \tag{2.3}$$

where m is mass of the particle, v is moving velocity, E is Young's modulus, Q is volume of the particle and σ is internal stress.

Required kinetic energy to break the particle is:

$$\frac{mv^2}{2} = \frac{\sigma_*^2}{2E}Q \qquad (2.4)$$

where σ_* is critical internal stress.

Arbiter (1969) studied and compared fractures of particles under low-velocity free-fall impact, double impact crushing and slow compression. He concluded that in all cases, for a sand-cement sphere, breakage started from the contact region. In free fall impact, the volume of permanent deformation was proportional to the energy input. Meridian fracture planes starting from the periphery of the circle of contact were developed by the wedging action of the cone of impact while oblique fracture planes were developed from the region around the cone following the trajectories of maximum compression. In slow compression and double impact crushing, breakage was caused by the wedging action of the cones and the hoop-tension existing in the peripheral part of the specimen. The sphere split into several spherical wedges together with the two cones.

Breakage of an Assemblage of Particles

Though the breakage of an assemblage of particles is more important in regard to the entire size reduction process, particle-bed studies received less atten-tion because a particle buried in a bed is difficult to retain in experimental control

For particle-bed studies, efforts were made to study the relationship between energy consumption and size reduction or new surface area created, and to study the mathematical simulation of the entire size reduction process.

ENERGY AND SIZE REDUCTION

Particle Size and Size Distribution

Prasher (1987) pointed out that any energy expenditure causing breakage must be related to the initial and final particle size conditions. For a single-particle, the initial size of the particle can be given by a number of ways. For an assemblage of particles, the initial size condition is usually a full distribution of sizes. In any case, the final condition or product will also be a complete size distribution.

Definitions of Individual Particle Size

There are basically three groups of definitions of irregularly shaped particle size (Prasher, 1987). The first group links the diameter of an equivalent sphere that would have the same property as the particle itself, as listed in Table 2.1. The second group of definitions use the diameter of a circle that would have the same property as the projected outline of the particles, as listed in Table 2.2. The third

group of definitions are associated with a linear dimension, as measured by a microscope, parallel to a fixed direction and may be classified as a statistical diameter, as given in Table 2.3.

Table 2.1 Definition of equivalent sphere diameters

Symbol	Diameter	Equivalent property of a sphere
x_V	Volume	Volume
x_S	Surface	Surface
x_{SV}	Surface/volume	Surface to volume ratio
x_D	Drag	Resistance to motion in the same fluid at the same velocity
x_{FF}	Free-fall	Free-falling speed in the same liquid with the same particle density
x_{ST}	Stokes	Free-falling speed if Stokes' law obeyed
x_A	Sieve	Passing through the same square sieve aperture

Table 2.2 Definition of equivalent circle diameters

Symbol	Diameter	Equivalent property of a circle
x_H	Heywood	Project area with particle resting in a stable position
x_P	Projected area	Project area with particle randomly orientated
x_C	Projected	Perimeter of the outline

Table 2.3 Definitions of statistical diameters

Symbol	Diameter	Equivalent property of a circle
x_F	Feret's	Distance between two tangents on opposite sides
x_M	Martin's	Length of the line dissecting the image of the particle
x_{SH}	Shear	particle width obtained with an image shearing microscope eyepiece
x_{CH}	Maximum chord	maximum length of a line limited by the contour of the particle

<u>Size Distribution</u>

Particle size distribution can be measured by number, mass, volume or surface. Size distribution by mass is the most commonly used method. It may be expressed in frequency form or cumulative form. Frequency form presents the mass of particles of each given size. Cumulative form presents the mass of particles over or under a given size. Therefore, the frequency is the derivative of the cumulative. Both frequency and cumulative forms can be plotted or expressed by mathematical functions. A wide range of mathematical functions have been used. An example of simple mathematical function to describe size distribution data in cumulative form is shown in Equation (2.5) (Rosin, 1933):

$$F(x) = 1 - e^{(-x/x')^{n'}} \qquad (2.5)$$

where x is particle size, x' is reference particle size and n' is uniformity index,

16

More complex functions such as log-normal distribution were sometimes used, as shown in Equation (2.6) (Prasher, 1987):

$$\frac{dF}{dx} = \frac{1}{2\sqrt{2\pi}}e^{(-\frac{x-x_a}{2\sigma^2})}$$ (2.6)

where x particle size, x_a is the arithmetic mean and σ is standard deviation.

The complexity of the size distribution problem calls for a system which is flexible enough to be tailored to any breakage pattern, and Broadbent and Callcott (1956a,b) found a powerful answer in vector and matrix algebra which has been extensively adopted in a modified form. Comminution starts with a feed of a certain size distribution and ends with a product of different size distribution. Each of the distributions is generally sized by sieving, the aperture sizes of which normally form a geometric progression. Thus, either feed size distribution or product size distribution is a list of the masses of particles of each aperture size. The feed and product lists can be regarded as column vectors and denoted by {F} and {P}, respectively.

Particle Surface

In the energy approach to study the comminution process, it is essential to understand the relationship between energy input and new surface energy. Therefore, measurement of surface area of a particle is of importance. There are a

17

number of available methods to determine the specific surface (surface area per unit mass of particles), such as air permeability, gas adsorption, photosedimentometry and laser granulometry, listed by Prasher (1987). However, specific surface is usually calculated from the particle size distribution. For any given size and shape of particles, specific surface can be calculated by mathematical means. For an assemblage of particles with irregular shapes, the relationship between the specific surface and particle size is determined by experiments.

Definitions of Energy for Breakage

Only a part of externally applied energy is used for breakage. It is important to distinguish applied energy and comminution energy. Comminution energy per unit mass, E, is actually used in size reduction and E_a is externally applied energy per unit mass. E_a is greater than E because many particles will be stressed to levels below the critical for fracture and the associated energy is lost as heat. Friction and other losses are also considerable (Prasher, 1987). A more useful concept about comminution energy is the utilization of energy, defined as new surface produced per unit of applied energy for a unit mass of material, $\Delta S/E_A$.

Energy and Size Reduction

The general relationship between size reduction and energy consumed is expressed in the following equation (Prasher, 1987):

$$dE = -K\frac{dx}{x^n} \qquad (2.7)$$

where E is the energy consumed to size reduction, x is the size of particle, K and n are constants. This equation suggests that the energy consumed be directly proportional to size reduction and inversely proportional to the original size of particles. Though various works have given different interpretations of this relationship (lynch 1977), it is difficult to apply this relationship to practical problem. The reason is that not all of the energy consumed is used to break particles. A large amount of energy loss occurs during the process, for example, energy loss in machine transmission, in friction, in elastic and plastic deformation, and in producing noise. Energy actually consumed in size reduction is hard to determine.

Energy and New Surface Area

Another approach to study energy law in size reduction is to find the relationship between energy consumed and new surface area created. The following equations were used by some researchers:

19

Kick's Law (Prasher, 1987)

$$\frac{\Delta s}{E_A} = \frac{K_4}{E_A x_1}[e^{(E_A/K_3)} - 1]$$ (2.8)

where, Δs is increase in mass-related specific surface, x_1 is feed size, E_A is statistical average mass-related specific energy and K_3 and K_4 are constants;

Bond's law (Bond, 1952)

$$\frac{\Delta s}{E_A} = \frac{1}{K_6}(E_A) + \frac{1}{K_7}(\frac{1}{\sqrt{x_1}})$$ (2.9)

where K_6 and K_7 are constants.

MATHEMATICAL SIMULATION OF SIZE REDUCTION PROCESS

In the comminution process, coarse material of a whole range of particle sizes is fed into a mill followed by successive comminution events. In this process when particles of a given material, geometry and size are individually stressed to a predetermined maximum level under predetermined conditions, some break and some do not. The ratio of the broken particles to the stressed particles is known as breakage probability. those particles which break yield smaller particles, known as product. the product of breakage varies widely, depending on characteristic size distribution. Based on the concepts of probability of breakage and characteristic

20

size distribution, two kinds of models are usually used to describe the repetitive process. These models are matrix models and kinetic models. In a matrix model, the comminution process is considered as a succession of selections and breakages. After subjecting a succession of selections and breakages, the feed {F} yields product {P}, as expressed in Equation (2.10):

$$\{P\} = ([B][S] + ([I] - [S]))\{F\} \tag{2.10}$$

where [B] is breakage distribution function, [S] is select function, and [I] is a unit matrix (Lynch, 1977).

The select function is affected by the size of particle, grinding time, mill speed, mill geometry, material property. The breakage distribution function depends on size distribution characteristics and mill variables.

In a kinetic model, the process of comminution is usually considered as a continuous process as shown in Equation (2.11):

$$\frac{dW(D)}{dt} = -k(D)W(D) \tag{2.11}$$

where W(D) is the weight of particles of size D, k(D) is rate constant of size D (Lynch, 1977). The main difficulty in the application of the continuous distribution model to practical problem in comminution is that of obtaining a satisfactory definition of the continuous function for the distribution of particle sizes.

Chapter 3
MECHANISMS OF REGRINDING AND DUST GENERATION

COMMINUTION MECHANISMS IN REGRINDING

The regrinding process in rotary coal cutting machines has been described as a interaction process between the cutting head and the mined coal material in a cutting path. Coal particles enter a circular cutting path from the place where they are mined and then are subjected to a complicated size reduction process in the cutting path. During this process, mined coal particles may experience secondary comminution by the following mechanisms:

Compression - When relatively large coal particles fall into a cutting path, the particles may be compressed between bit blocks and coal face, cutting drum and coal face.

Impact - Bits and bit blocks on a rotating cutting head impact coal particles, forcing them to move or throwing them into air. The moving particles impact one another and impact surrounding objects, resulting in impact breakage.

Attrition - During the transit of mined coal material through a cutting path, coal particles impact each other slightly. Some particles roll or slide on the surface of others. As a result, a very thin layer of material is removed from the surface of coal

22

particles.

Each of the comminution mechanisms will generate coal dust. To answer the question of how the secondary comminution generates dust, the principles of compression, impact, attrition and resulting dust generation have been investigated theoretically and experimentally, and are described as follows.

COMPRESSION AND DUST GENERATION

When a rotary cutting head cuts coal, it rotates and advances simultaneously. The advancement of the cutting head alters the space between the cutting head and coal face. The maximum space immediately follows the cut. This space reduces gradually as the continuous miner advances and reaches the minimum space immediately before the cut. The change in the space between the cutting head and the coal face is equal to the depth of cut. The coal particles mined from the coal seam and falling into the cutting path could be compressed and crushed because of the change in the space of the cutting path. The rotating action of the cutting head could also crush the coal particles in the cutting path.

The principles and failure patterns associated with compression have been studied extensively (Prasher, 1987). Prasher pointed out that under two or more compressive forces, cracks developed from any one contact point in the direction of another force contact point and form a wedge or cone shape crushed zone under each

23

force contact point. However, dust product resulting from compressive crushing failure was seldom discussed. In order to study dust generation due to compression, compressive crushing failure was further investigated experimentally and analytically and is discussed in the following sections.

Experimental Investigations

Circular disc rock specimens and coal specimens were crushed by an electro-hydraulic testing machine (MTS), according to the schematics of Figure 3.1. The specimens had a diameter of 7.62 cm and a thickness of 2.54 cm. The process of compressive crushing was controlled by programming the rate of crushing displacement. The rate was set to 0.00025 cm/s, with the option of holding machine displacement at any level during the test. Thus, the progress of crushing failure could be observed stage by stage.
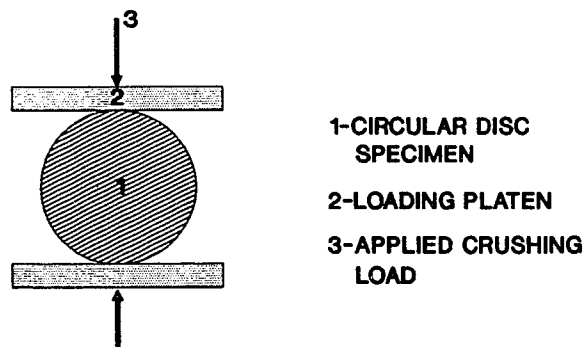
Figure 3.1. Illustration of compressive crushing test

Four characterized stages were observed in the process of slow compressive crushing, as shown in Figures 3.2a-d. Figure 3.3 presents the relationship between compressive force and displacement in each stage of the process. The characteristics of the failure and load-displacement relationship in each stage are discussed as follows.

The first stage includes formation of the primary fracture. In this stage, applied load increased with displacement until a fracture initiated at the center of the disc, which is known as primary fracture. Then, the fracture propagated rapidly to join the two contact points, splitting the specimen into two semi-circular discs, as shown in Figure 3.2a. The applied load dropped suddenly with the initiation and propagation of the primary fracture (see Figure 3.3). A small amount of dust and fine particles was observed during the primary fracture development.

The second stage includes formation of the secondary fractures. In this stage, the primary fracture opened gradually with further crushing displacement. The contact areas between the disc and loading platens increased. The applied load also increased with crushing displacement. Subsequently, when the load increased to 50% of the ultimate load, secondary fractures formed and were accompanied with a little load drop. The secondary fractures initiated near the contact areas and propagated in an angle to intersect the primary fracture and to form a wedge, which is called crushed zone, as shown in Figure 3.2b.

The third stage includes development or growth of the secondary fractures and

25

the crushed zone. In this stage, a group of secondary fractures appeared and the size of crushed zone increased with the crushing displacement. The stresses within the wedge were released and some crushed materials were separated from the specimen, as shown in Figure 3.2c. In this stage, the crushing load increased with further displacement.

The fourth stage includes growth of the crushing zone and collapse of the specimen. In this stage, the size of wedge increased with further crushing. The wedge was forced to move toward the center of the specimen, and the primary fracture opened to the limit, causing the specimen to become unstable and collapse, as shown in Figure 3.2d. Fine material debris accumulating on the loading platen gradually increased from the first stage to the fourth stage. But the amount of fine particles and dust was not significant. However, a significant amount of dust and fine particles were released from the crushed zone when the specimen collapsed.
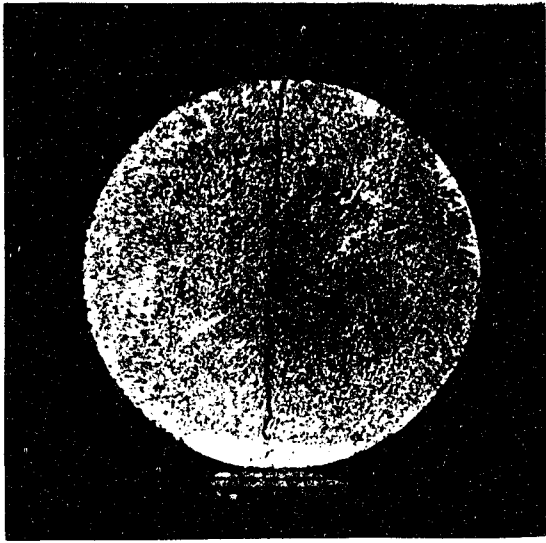
a) Formation of primary fracture
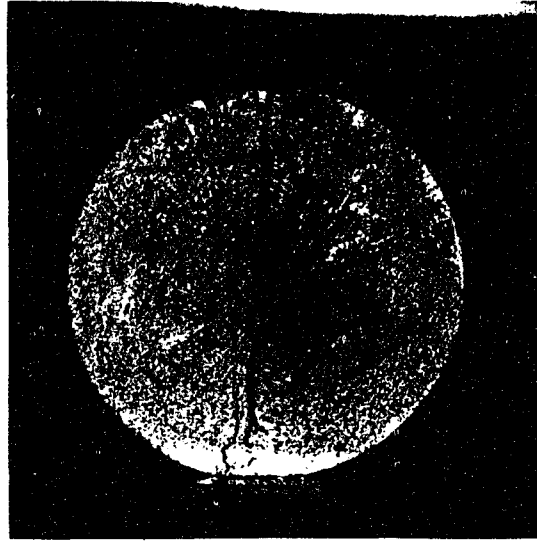
b) Formation of secondary fractures
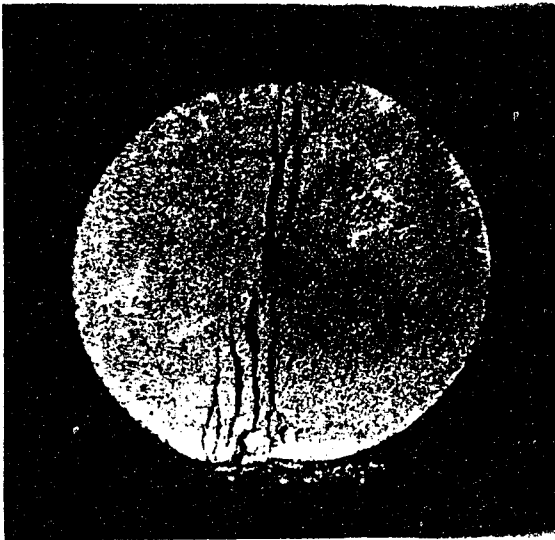
c) Growth of wedge size
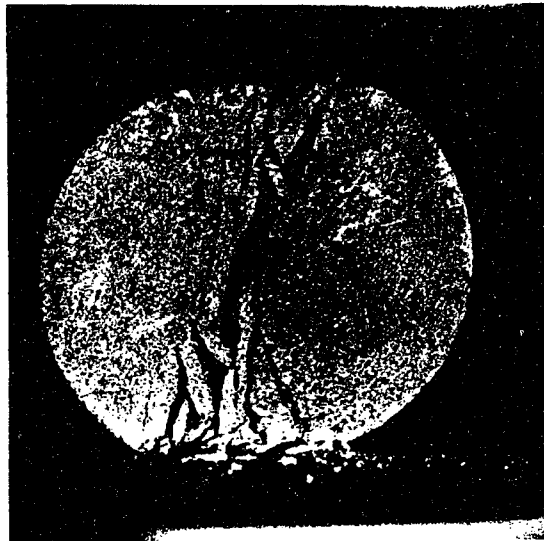
d) Unstable, near collapse specimen

Figure 3.2 The process of a slow compressive crushing
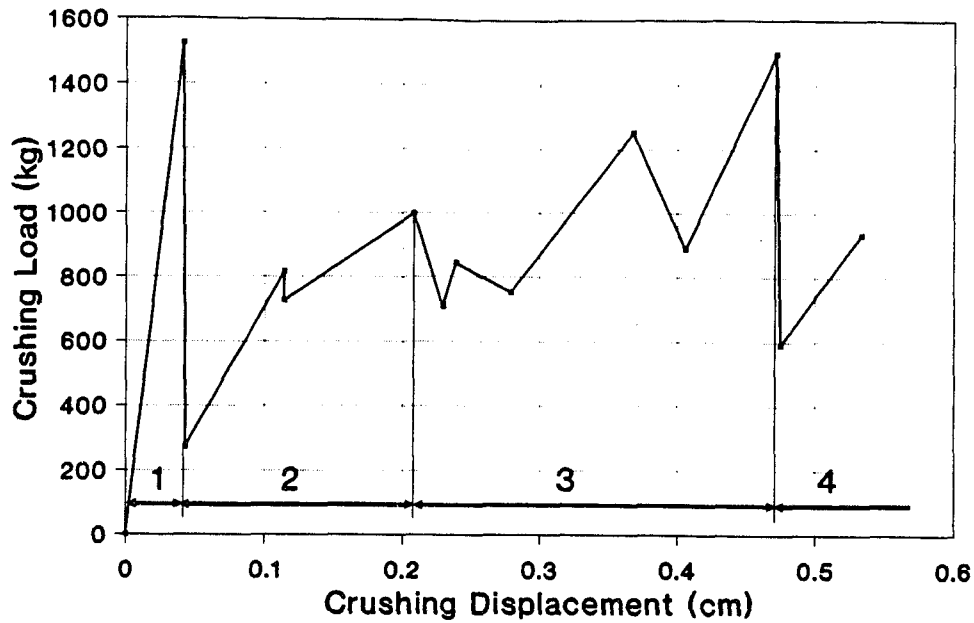
Figure 3.3. Relationship between compressive force and crushing
displacement in each stage of the crushing process
(Indiana limestone, disc specimen)

The size and shape of the crushed wedges developed in the fracture zone

depend on a number of factors. The greater the magnitude of crushing displacement

is, the larger the wedge size will be. Material properties also affect the size of the

wedges. For a hard material, which has a higher strength, the secondary fractures are

often parallel to the primary fracture, forming a fractured strip from one contact point

to another instead of two crushed wedges. High strain energy release from hard

specimen during the development of the primary fracture usually results in a burst,

throwing away the specimen from its loading alignment and keeping it from further crushing. In this case, small wedges are expected. For a soft material, because less strain energy releases during the formation of the primary fracture, the specimen remains aligned with its loading direction, in a position to be subjected to further crushing. Under the latter situation, development of a higher plastic deformation in the fractured zones and formation of larger wedges are expected.

Failure characteristics within the wedges also depend on material properties. Soft materials fail and smash, yielding fine and even size of particles. Strong materials yield some relatively large size particles and some very fine particles.

The magnitude of fine particles and dust generated during the development of the primary fracture and wedge formation depends on material property. It seems that hard materials produce more dust and fines on the loading platen, as shown in Figure 3.4. This certainly does not mean that more fine particles and dust are generated by crushing hard materials than soft materials, because a soft material might keep its dust from flying or becoming airborne. But it is certain that hard materials yield smaller size of dust and fine particles than soft materials when they are crushed.
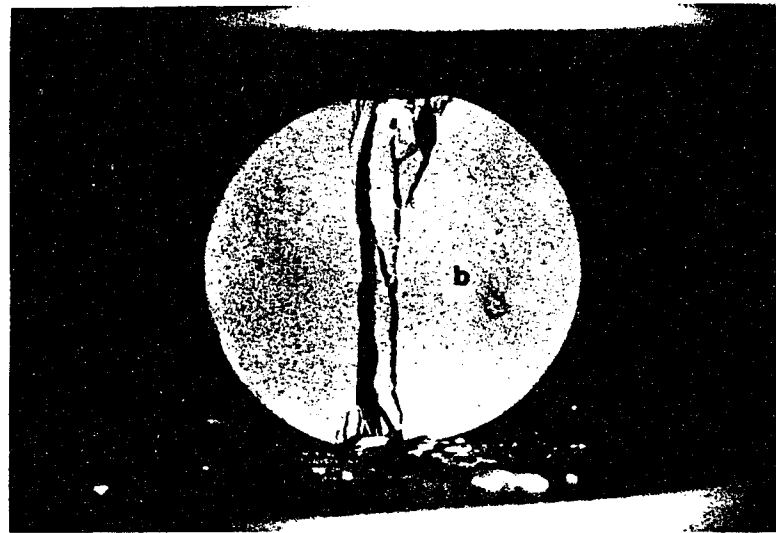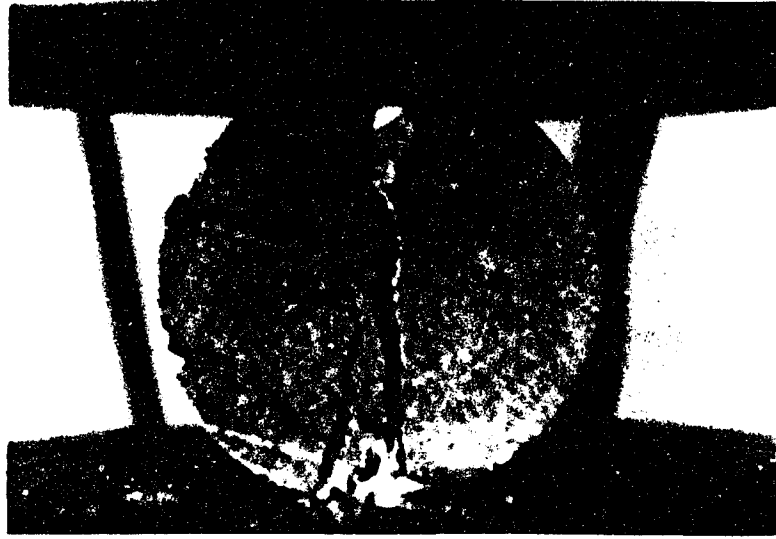
Figure 3.4. Effect of rock properties on compressive crushing failure
a) Indiana limestone, compressive strength σ_c=253 kg/cm^2,
b) Berea sandstone, σ_c=610 kg/cm^2

Coal specimens contain three groups of cleats. When load was applied along main cleats, primary fracture and secondary fractures initiated and propagated along the cleats. Wedges did not always exist, as shown in Figure 3.5. In this case, less dust and fine particles were generated since it did not require much energy to open the cleat. When load was applied to the specimen in the direction perpendicular to the main cleat, primary fracture formed in the direction of load and was followed by a secondary fracture along the main cleat, splitting the specimen into four quarters as shown in Figure 3.6. To consider different shapes of specimens, irregularly shaped specimens and cubic specimens were tested. For an irregularly shaped specimen, the protruding parts were crushed first because of a high stress concentration and were accompanied with fine dust particles, as shown in Figure 3.7. Following the crushing of protruding parts, the entire specimen was broken into pieces. For a cubic specimen, crushing load was uniformly applied to the surface area and the specimen broke into uniform medium size and fine product (see Figure 3.8). This observation reveals that the level of stress concentration and stress state could play a key role in the dust generation during compression. A high level of stress concentration and a complex stress state will fail/smash the material into very fine products.
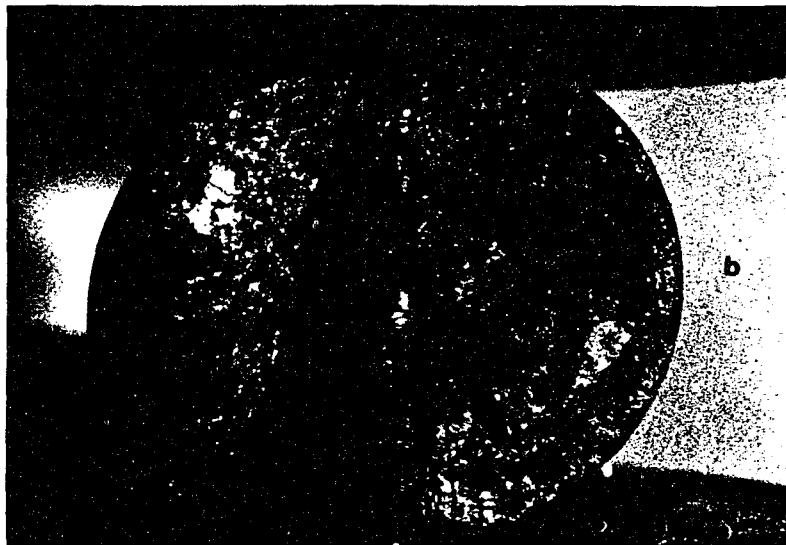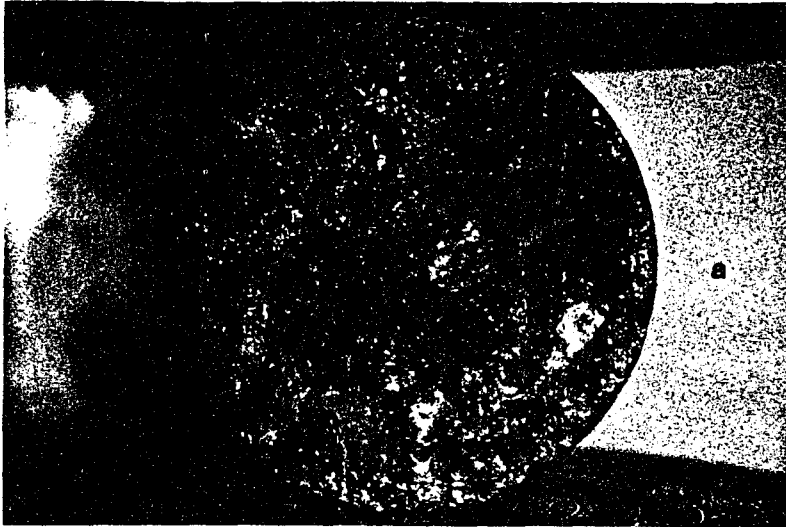
Figure 3.5. Compressive crushing of coal specimen along face cleats
a) Fracture initiation stage, b) Collapse stage
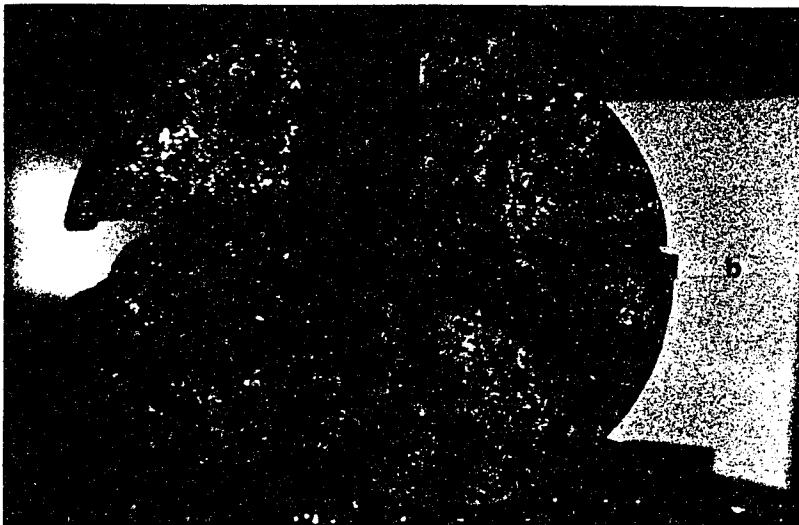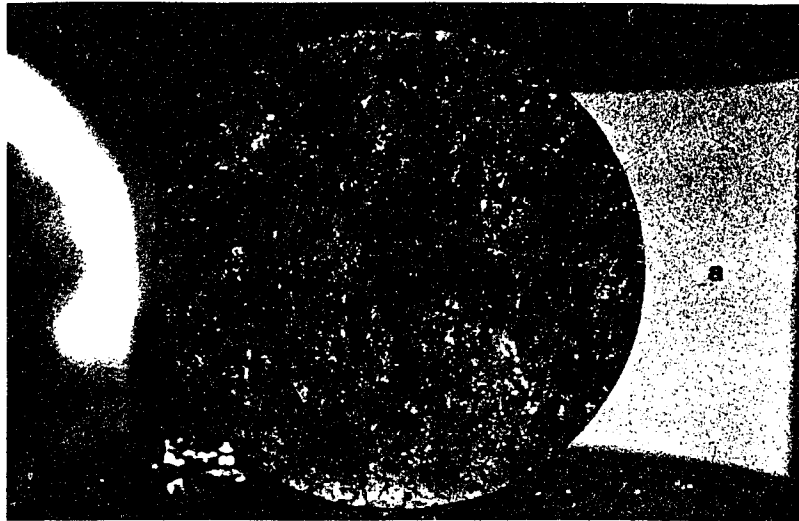
Figure 3.6. Compressive crushing of coal specimen along butt cleats
a) Fracture initiation stage, b) Collapse stage

33
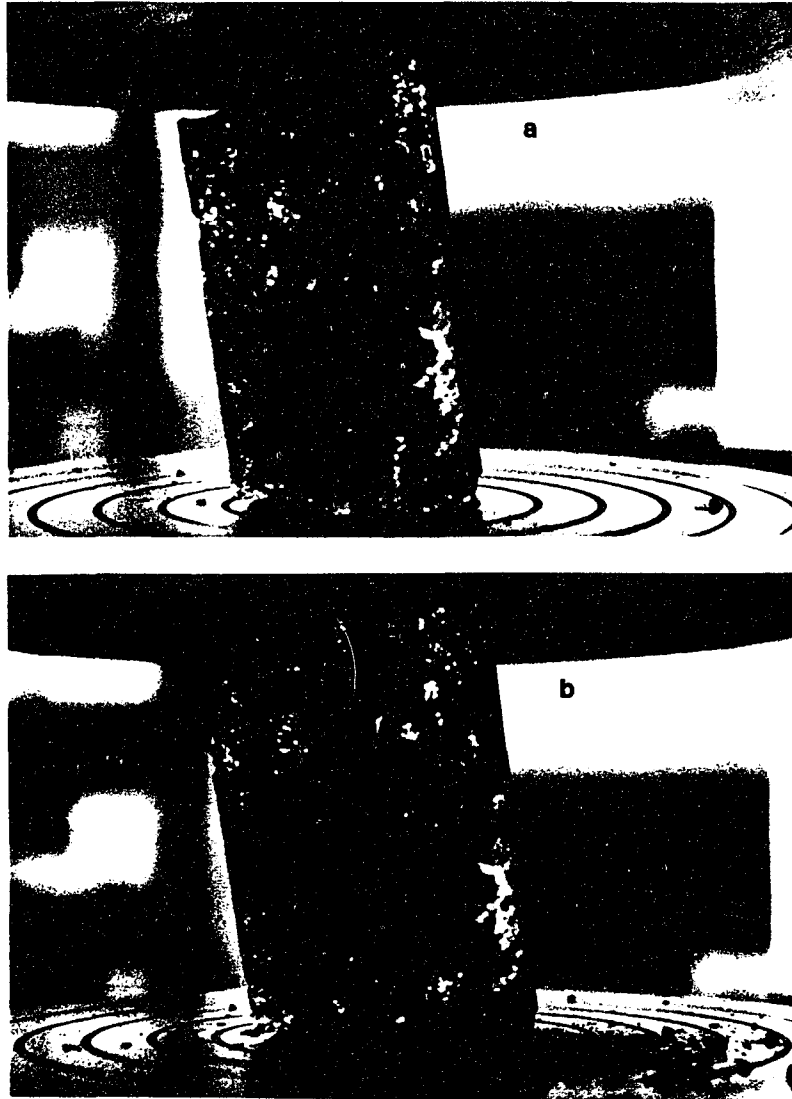
Figure 3.7. Compressive crushing of irregularly shaped coal specimen
a) Crushing of protruding parts, b) Crushing of entire specimen

34
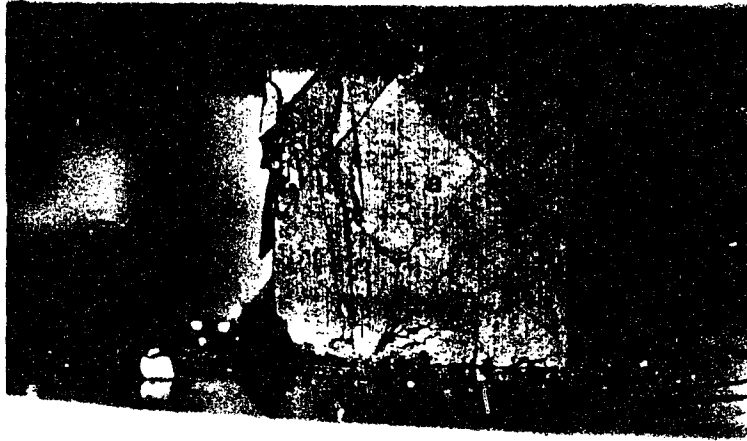
Figure 3.8. Compressive crushing of cubical coal specimen
a) Failure stage, b) Collapse stage

Finite Element Analysis

In order to study the stress pattern within a specimen subjected to compressive crushing, finite element technique was used to simulate the crushing experiments as described above. A disc specimen with a diameter of 2.54 cm and a thickness of one quarter of the diameter was compressed with two equal and opposite forces along the diameter AB as shown in Figure 3.9. The following parameters were assumed for the material: a Young's modulus of 42194 kg/cm^2, a Poisson's ratio of 0.3, and an acting force of 99 kg.
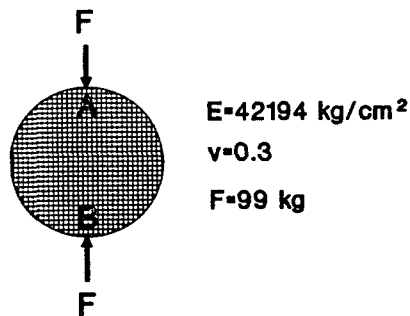
Figure 3.9. Finite element model to study compressive crushing stress pattern

A finite element program, NASTRAN, was utilized to study this problem. Tensile stress and compressive stress distributions were obtained as shown in Figures 3.10-11. Since the model is symmetric in both x-axis and y-axis, stress distribution diagrams were presented only for a quarter of the specimen.
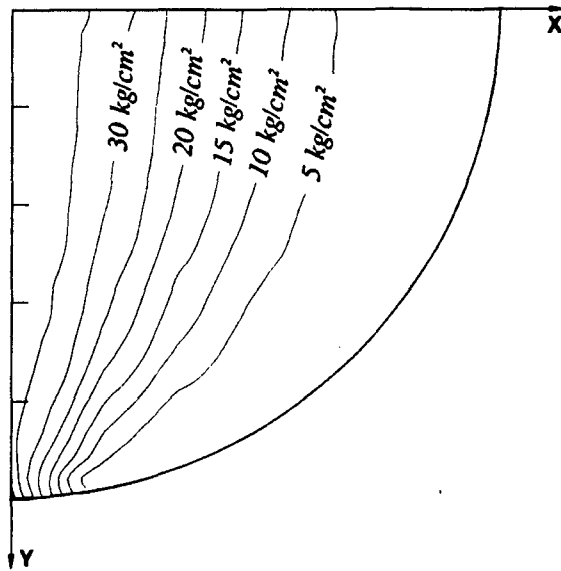
Figure 3.10. Major principal stress distribution (tensile stress)
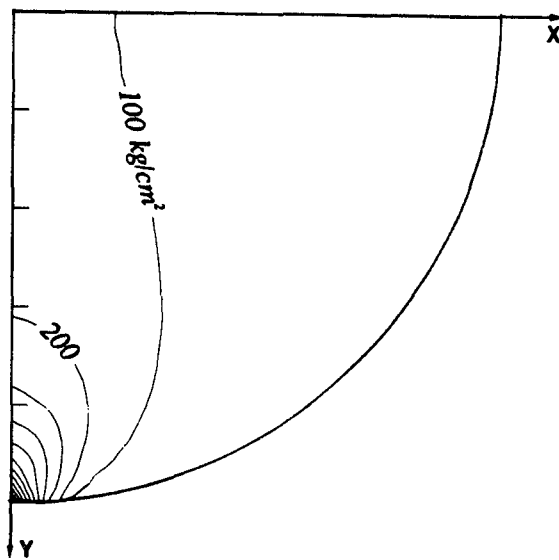
Figure 3.11. Minor principal stress distribution (compressive stress)

Figure 3.10 shows the major principal stress pattern. It indicates that the maximum tensile stress occurs around the contact point and it is $80°$ to x-axis. Crack may initiate around the contact point. But this crack will not go deep because this area is confined by high compressive stresses, and the tensile stress surrounding this zone is relatively low. Therefore, it can be considered as a local tensile stress pattern and it does not determine global failure. Global tensile stress pattern is characterized by high tensile stresses along the diameter AB which joins the contact points. The tensile stress at the center is parallel to the x-axis or perpendicular to the loading direction. The direction of tensile stress along diameter AB changes slightly from $0°$ at center to $8°$ near the contact area with regard to the x-axis, This global tensile stress pattern shows that a crack is likely to initiate and open up at the center because of the magnitude and direction of the tensile stress. This crack easily propagates to join two contact points because of the high tensile stresses along the diameter AB of the specimen. Figure 3.11 shows that high compressive stress concentration exists near the contact area. Because of the high stress concentration, the material under the contact point will be crushed. The volume of crushed zone is an important parameter in evaluating dust generation due to crushing failure. Using Von Mises stress criterion (or maximum distortion energy criterion), the volume of the crushed zone, or plastic failure zone, can be determined as shown in Figure 3.12. Based on finite element analysis, it can be inferred that the primary crushing failure includes a major crack

along the diameter joining two contact points, accompanied with two compressive failure zones or crushed zones right under the contact points. Stresses in the crushed zone are released. If the crushing continues after primary failure, the major crack will open up and the size of the crushed zones increase, forming a wedge shape crushed zone as observed in the laboratory experiments.
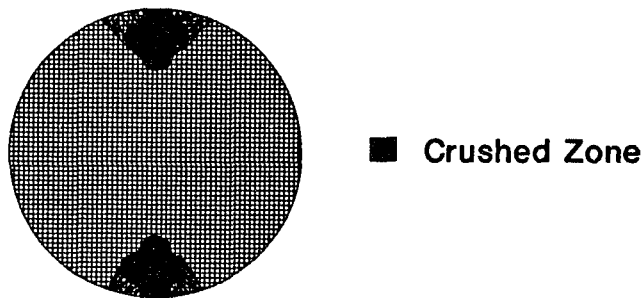
■ Crushed Zone

Figure 3.12. Crushed zone due to compression, obtained by finite element analysis

IMPACT FAILURE AND DUST GENERATION

The characteristics of impact failure of coal particles in cutting path are similar to those in an impact mill. Bits and bit blocks impact coal particles by coming in contact with them. After coal particles become dynamic or flying, they impact one another and impact surrounding objects. These impact events result in impact failure and generate dust. When a moving particle impacts an object, high impact force is created on contact point and inertia force is raised in the particle because of sudden

39

deceleration. Under the influence of these two forces, internal stresses are produced in the particle. Cracks initiate near the contact point and propagate outwards from the contact area. This process was observed stage by stage in laboratory using a high speed video camera. Figure 3.13 shows the result from a free-fall experiment in which irregularly shaped coal particles impacted a metal plate. The surfaces of coal particles were painted white so that fractures could be seen clearly. The fracture patterns can be seen clearly in the area away from the contact point. Near the contact area, a void develops. Based on the observation of free fall impact in laboratory, it was found that the material originally occupied the void was crushed and the crushed material was thrown away or became airborne. A great portion of the crushed material in the void became dust. Therefore, determining the volume of the crushed zone is an indirect evaluation of dust generation due to impact failure. The objective of impact failure study was to determine the volume of crushed zone by internal stress analysis and energy transformation analysis.

Figure 3.13 Typical impact failure

Finite Element Analysis of the Impact Failure

In order to study impact failure and determine the volume of the crushed zone, a dynamic finite element method, transient response, was employed to study the internal stresses and failure caused by impact. A model consisting of a disc coal specimen impacting semi-infinite rigid body, as shown in Figure 3.14, was utilized to simulate free fall impact.
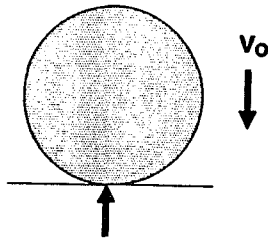
Figure 3.14 Free fall impact model for finite element analysis

The dynamic governing equation, initial conditions and boundary conditions for This model are as follows:

$$[M]\{\frac{d^2\delta}{dt^2}\} + [K]\{\delta\} = 0 \tag{3.1}$$

and initial condition and boundary conditions

$$\frac{d\delta}{dt} = 0 \qquad at \ t=0$$

$$\delta = 0 \qquad on \ contact \ area \tag{3.2}$$

where [M] is mass matrix, [K] is stiffness matrix, $\{\delta\}$ is displacement vector.

41

Assuming that the thickness of the disc is one quarter of its diameter and all required parameters, such as initial velocity, Young's modulus and Poisson's ratio, are given, utilizing a computer program, NASTRAN, the impact force on the contact point, the deceleration, velocity, displacement and stress distribution within the specimen during impact period were obtained.

For example, for the given conditions such as: a diameter of 2.54 cm (D=2.54 cm), an initial velocity of 4 m/s (v_0=4 m/s), a Young's modulus of 42194 kg/cm^2 (E=42194 kg/cm^2) and a Poisson's ratio of 0.3 (v=0.3), the velocity and displacement during impact period were determined as shown in Figures 3.15-16. Figure 3.15 shows how the velocity within the body changes during the impact period. The result indicates that when a coal particle impacts a rigid body at an initial velocity of 4 m/s, the velocity of the particle drops to zero within 42 microseconds. The velocity at point 1, near the contact area, drops rapidly while the velocity at point 2, at the center, decreases slowly at the beginning. However, the velocities at both points reduce to zero almost at the same time.

Figure 3.16 shows that displacement of point 1, at the center, is almost equal to that of point 2, at the far side from contact point. This result indicates that the deformation is severe near the contact area but it is slight beyond the center point.
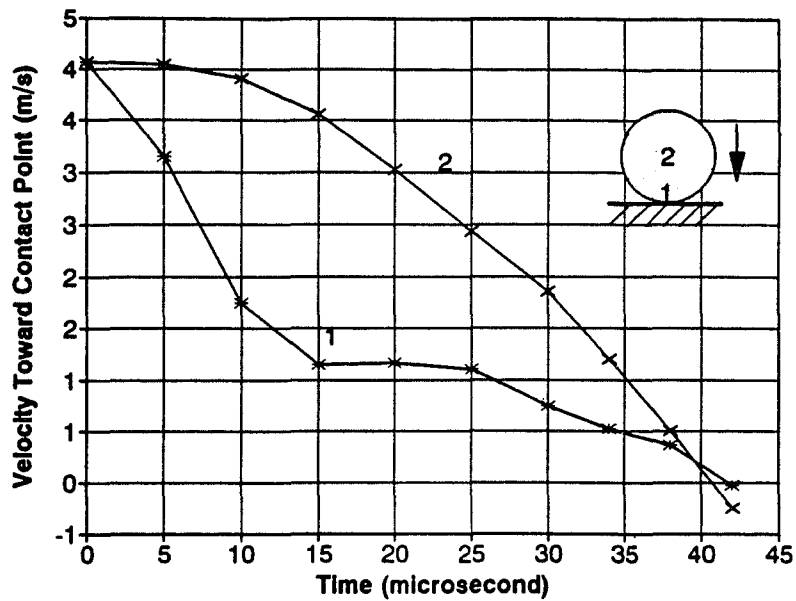
Figure 3.15. Velocity at nodal points of 1 and 2 during the impact period
(D=2.54 cm, E=42194 kg/cm^2, ν=0.3)
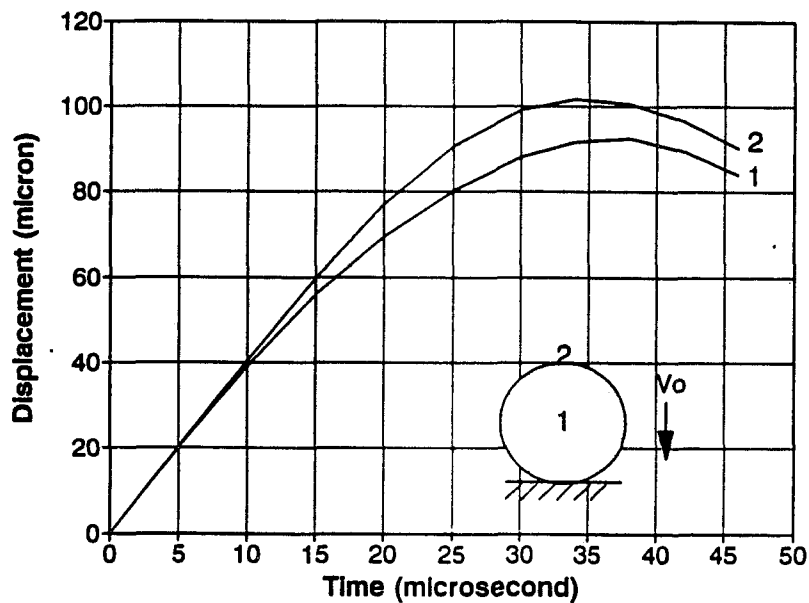
Figure 3.16. Displacement at nodal points of 1 and 2 during the impact period
(D=2.54 cm, E=42194 kg/cm^2, ν=0.3)

Impact force increases with time during the impact period, as shown in Figures 3.17a-c, and it reaches the maximum value when the velocity reduces to zero, and the displacement becomes maximum. The magnitude of impact force depends on the initial conditions, the size and the properties of the particles. Figure 3.17a shows the effect of Young's modulus on the impact force during impact period. A higher Young's modulus results in a greater impact force. Figure 3.17b shows that impact force increases with particle size and Figure 3.17c indicates that impact force is directly proportional to the initial impact velocity.
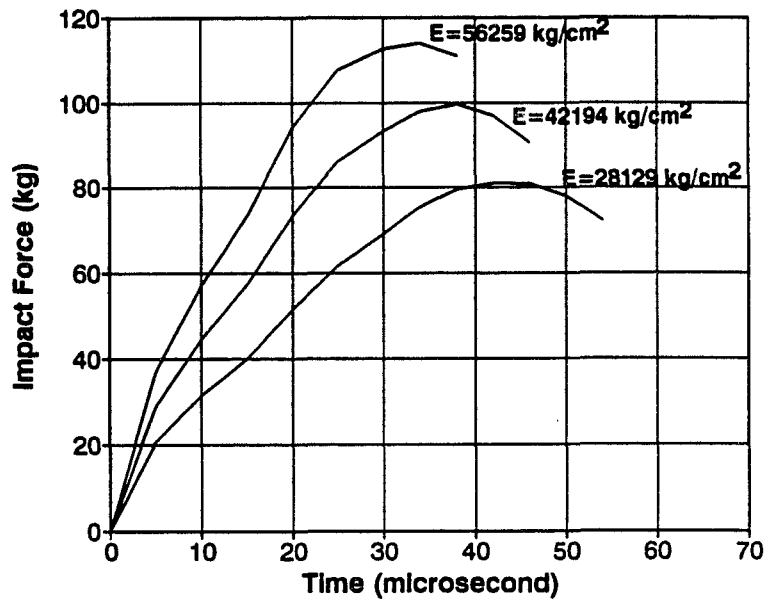
Figure 3.17a. Effect of Young's modulus on impact force during the impact period
(D=2.54 cm, v_0=4 m/s, and v=0.3)
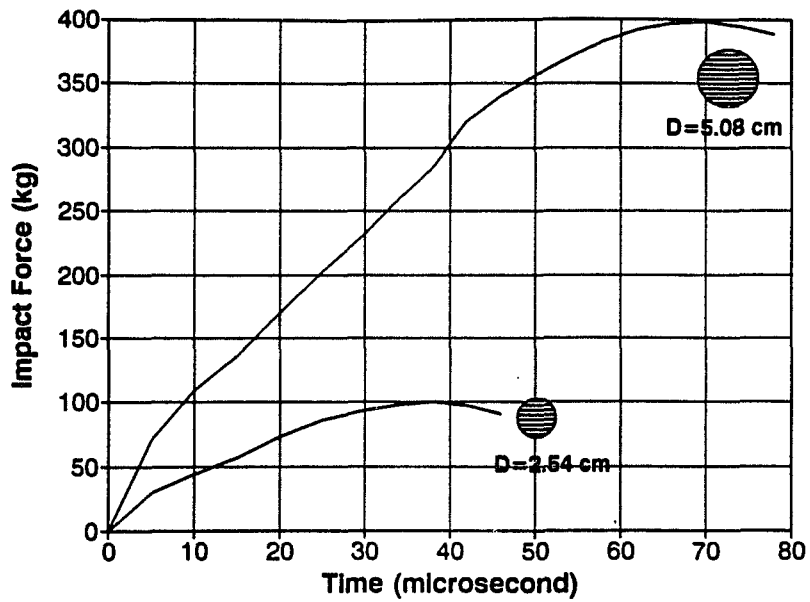
Figure 3.17b. Effect of particle size on impact force during the impact period
($E=42194$ kg/cm^2, $v_0=4$ m/s, and $v=0.3$)
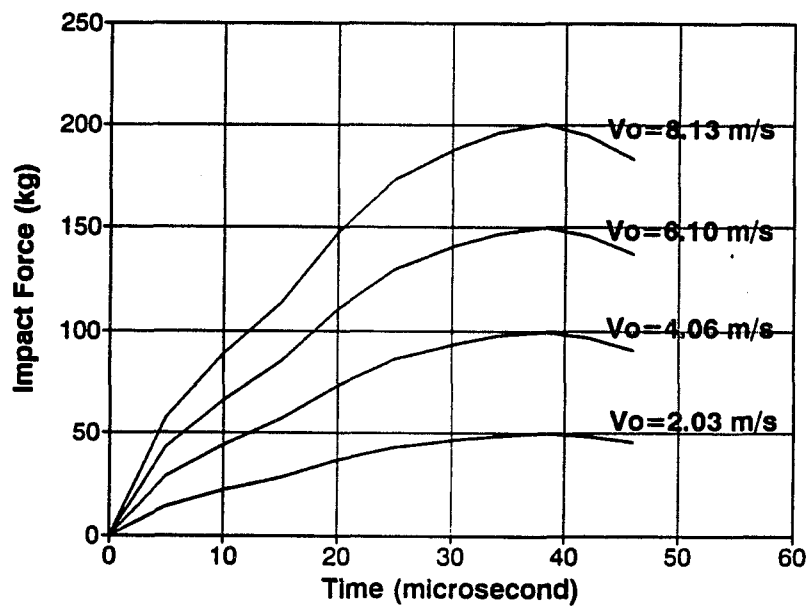
Figure 3.17c. Effect of initial velocity on impact force during the impact period
($D=2.54$ cm, $E=42194$ kg/cm^2, and $v=0.3$)

45

Figure 3.18 shows a typical internal stress distribution under the maximum impact force. High stress concentration occurs near the contact point. Stresses decrease rapidly in the body farther away from the contact area. Both compressive and tensile stresses are small at the center of the specimen.
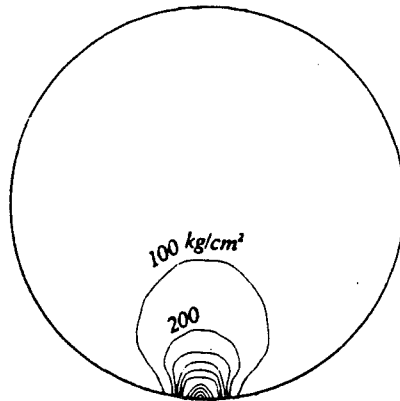
Figure 3.18. Minor principal stress (compressive stress) distribution under the maximum impact force, (D=2.54 cm, E=42194 kg/cm^2, v_0=4 m/s, v=0.3)

Because of the high compressive stress concentration near the contact point, a crushed zone will be created. The volume of crushing failure was determined utilizing the maximum distortion energy criterion. Figure 3.19 shows the process of the formation of the crushed zone. The crushing initiates at the contact point and then takes a step toward center point. The next step is toward both sides, and then step toward the center again. It takes about 30 microseconds to complete the development of the crushed zone. Then, the size of the crushed zone remains stable.

DEVELOPMENT OF CRUSHED ZONE

t = 5   t = 10   t = 20   t = 30   t = 40

■ Crushed Zone
Time t (microsecond)
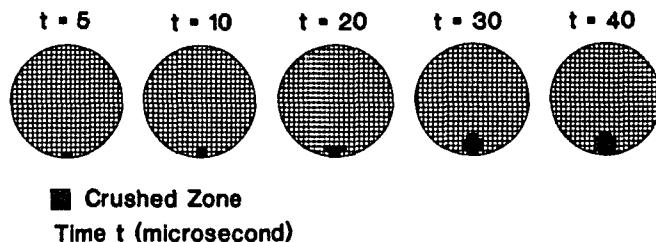
Figure 3.19. Process of formation of crushed volume

Final crushed volume depends on its initial condition and coal properties. For

a given initial condition and particle size, the volume of the crushed zone increases

with Young' modulus, as shown in Figure 3.20. Uniaxial compressive strength of coal

material has significant effect on crushed volume, as shown in Figure 3.21. For a given

initial impact velocity, when the strength of coal material is less than 282 kg/cm^2, the

volume of the crushed zone increases rapidly with further decrease in the strength of

coal material; when the strength of material is greater than 422 kg/cm^2, the volume

of the crushed zone does not significantly increase with further increase in the strength

of coal material. Figure 3.22 shows that initial velocity also has significant effect on

the volume of the crushed zone. For the given coal properties, if initial velocity is less

than 2 m/s, crushing may occur only on the surface. However, when the initial velocity

is greater than 2 m/s, the volume of the crushed zone increases rapidly with higher

47

initial velocity. Other parameters, such as Poisson's ratio and particle size, have less significant effect on the volume of the crushed zone. Although the volume of the crushed zone increases with particle size, the volume of the particle also increases with particle size. Thus, the crushed volume per unit volume of particle does not depend on the particle size. Poisson's ratio shows little effect on the crushed volume.
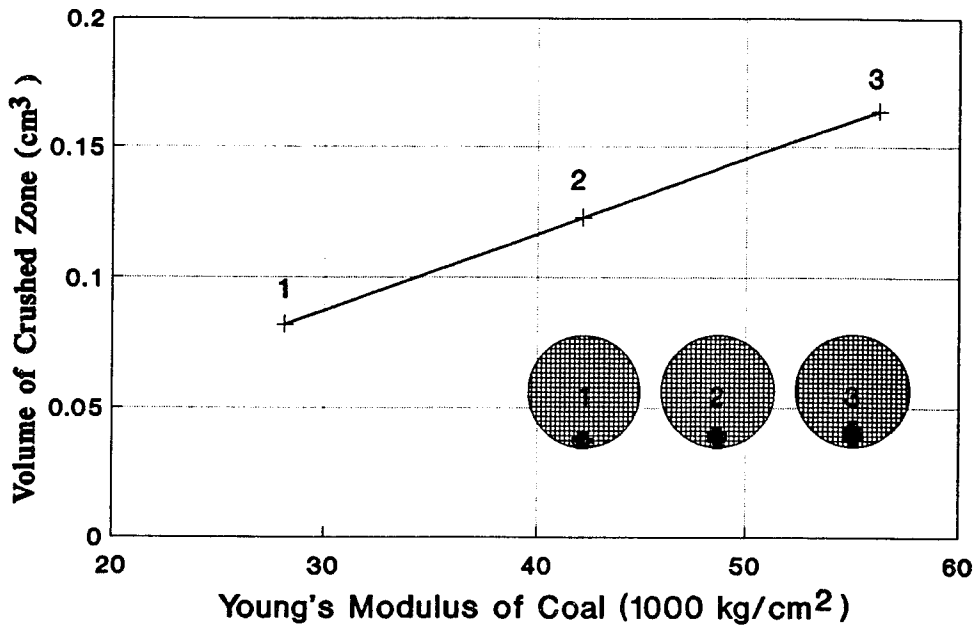
Figure 3.20. Effect of Young's modulus on the volume of the crushed zone
(σ_c=281 kg/cm^2, D=2.54 cm, and V$_o$=4 m/s)

48
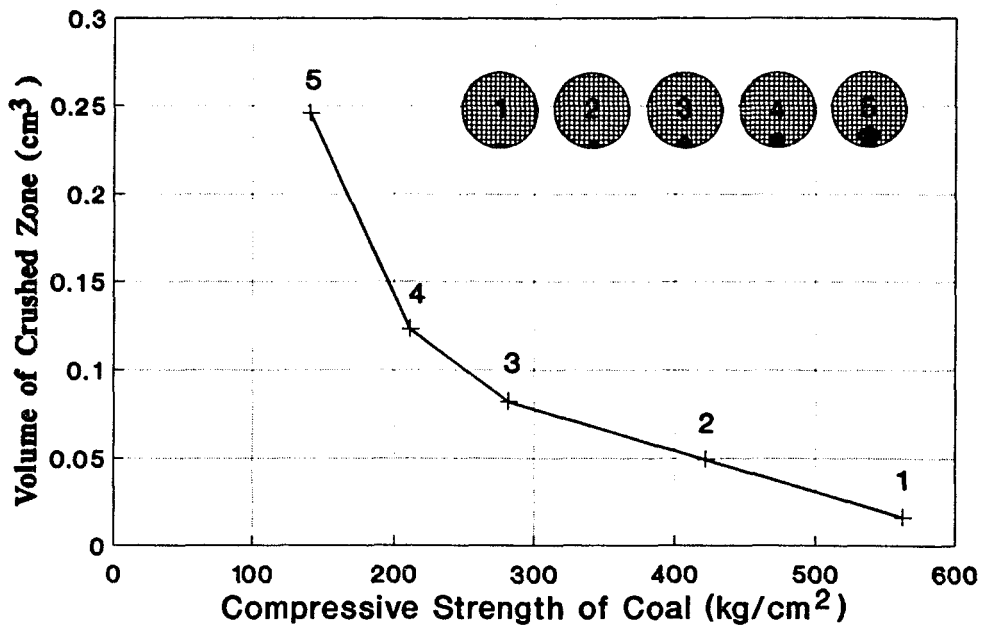
Figure 3.21. Effect of compressive strength on the volume of the crushed zone
($E=42194$ kg/cm^2, $D=2.54$ cm and $V_o=4$ m/s)
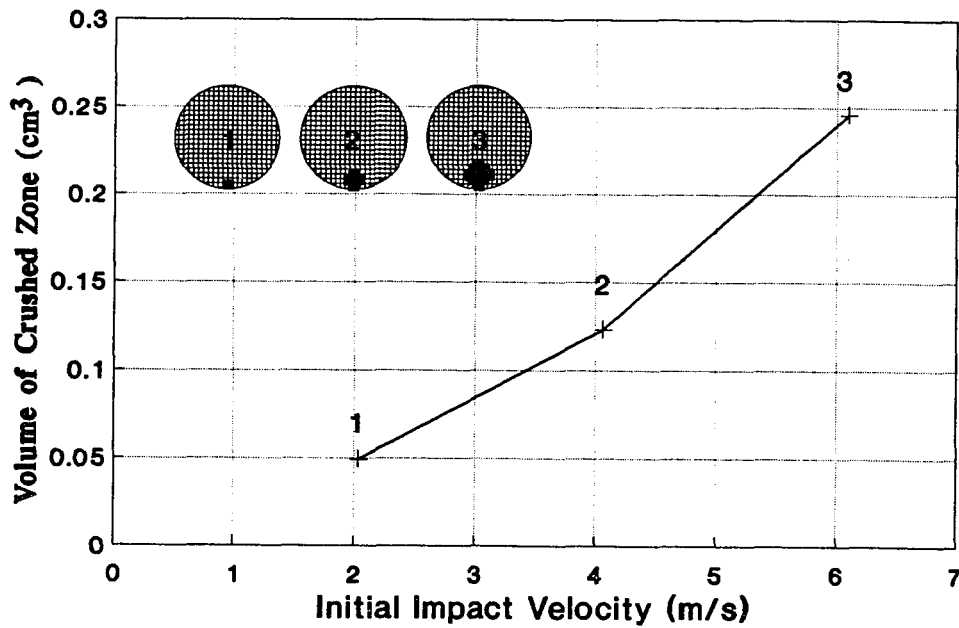
Figure 3.22. Effect of initial velocity on the volume of the crushed zone
($\sigma_c=281$ kg/cm^2, $E=42194$ kg/cm^2, $D=2.54$ cm)

Energy Transformation Analysis

The purpose of energy transformation analysis is to establish the relationship between the volume of crushed zone and input kinetic energy. Some definitions concerning energy transformation analysis are given as follows.

Kinetic energy - Assuming that a particle moves at a velocity of v_0, before the particle impacts an object, it has kinetic energy W such as:

$$W = \frac{1}{2}mv_0^2 \qquad (3.3)$$

where m is the mass and v_0 is the velocity of the particle.

Strain energy - Energy stored in a particle through elastic deformation and it is defined as:

$$W_s = \iiint_Q \frac{\sigma^2}{2E} dQ \qquad (3.4)$$

where σ is internal stress, Q is volume of the particle.

Utilized energy - The energy used to create crushed volume, also known as *crushing energy*.

Nominal specific energy - It is defined as the required kinetic energy input to create a unit volume of crushed zone and equals to the ratio of kinetic energy of a particle to the volume of the crushed zone in the particle.

Utilized specific energy - It is defined as the required crushing energy to create

50

a unit volume of crushed zone and equals to the ratio of crushing energy to the volume of the crushed zone.

During impact, the kinetic energy is transformed into internal strain energy. If energy transformation were perfect, the relationship between strain energy and kinetic energy would be as follows:

$$\frac{mv_0^2}{2} = \iiint_Q \frac{\sigma^2}{2E}dQ \tag{3.5}$$

During the impact, some of the strain energy is consumed in the formation of fractures, some of the energy is utilized to crush the material, forming a crushed zone, and the rest of the energy is released, resulting in bounce of particle or heat formation. Therefore, only a portion of total internal strain energy or kinetic energy is utilized to create the crushed zone. This portion of the energy is known as crushing energy. Based on finite element analysis of the problem, it was found that the ratio of crushing energy to total strain energy, known as energy ratio, decreased as the strength of material increased, as shown in Figure 3.23. This result indicates that in soft materials, most of the kinetic energy is utilized to create crushed zone while in hard materials, less kinetic energy is used to create crushed zone. Hence, more strain energy is released during the impact of hard materials, resulting in a larger bounce distance.
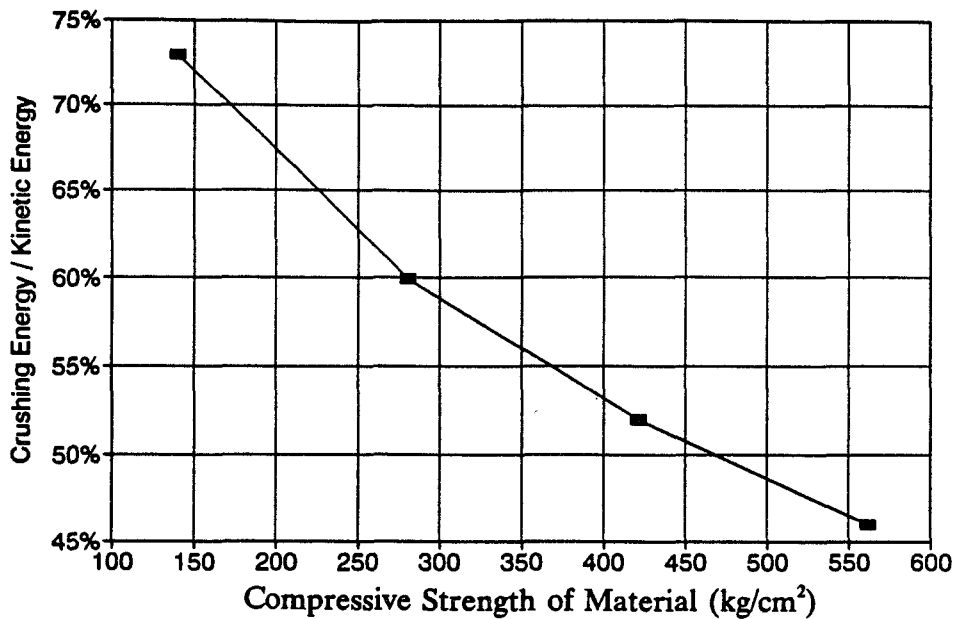
Figure 3.23. Relationship between energy ratio and material properties

Utilizing the results of the finite element analysis, nominal specific energy and utilized specific energy were determined. Magnitudes of both nominal specific energy and utilized specific energy are dependent on the material properties as shown in Figure 3.24. Nominal specific energy is always greater than utilized specific energy since only a portion of total strain energy is consumed to crush the material. With the help of these two indices, the crushed volume can be evaluated for a given initial condition and material properties.
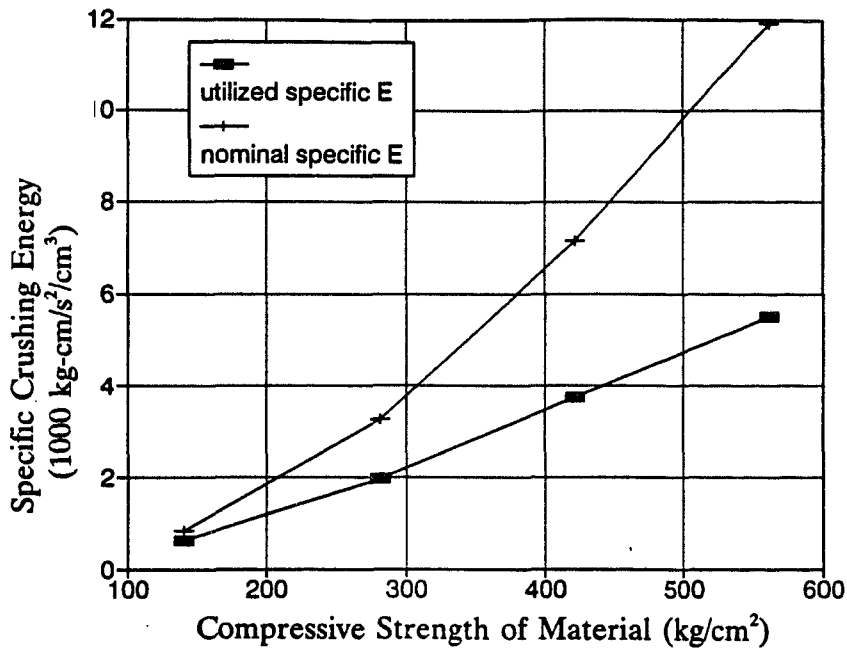
Figure 3.24. Nominal specific energy and utilized specific energy
with varied compressive strength of material

ATTRITION AND DUST GENERATION

A coal seam is composed principally of macerals and subordinately of minerals.

The structure of coal can be considered as tiny graphitelike layers packed in a

turbostratic, or random-layer-lattice. In this structure, successive layers are stacked

roughly parallel to each other, and megascopic and microscopic porosities and cleats

are present. When coal is broken, the surface of coal particles is a very rough surface

because of the turbostratic, porous and cleavage structure as shown in Figure 3.25.

The level of asperities depends on the rank of coal. When coal particles impact one

53

another at a very low velocity or slide on a surface of other objects, the asperities on the surface will fail under high local stresses, even though the total impact force is very small. The failure is in microscopic scale and is invisible. As a result of this failure, a very thin surface layer is removed from the particles. The loss of surface layer is known as attrition. Attrition has the most significant contribution to airborne dust generation during regrinding because every coal particle will be subjected to attrition during their transit through cutting path and the product of attrition has a particle size of less than 10 microns.
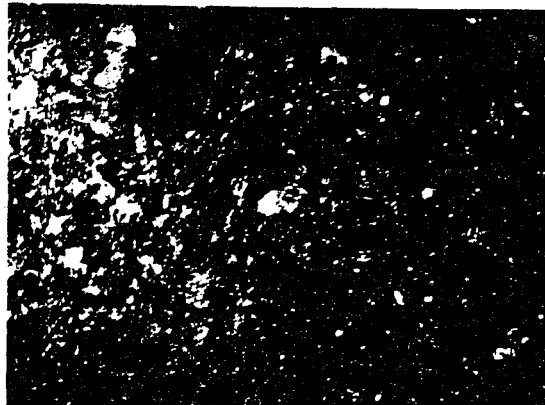
Figure 3.25. Surface characteristics of coal particle magnified (x100)

In the cutting path, attrition of coal particles is caused by contact action, sliding or rolling. The principles and results of each action were studied and discussed as follows.

Attrition due to Contact Action

Assuming that a spherical particle with a diameter of R_2, a mass of m_2, a Young's modulus of E_2, and a Poisson's ratio of v_2, at a low velocity of v_0, contacts a semi-infinite body, which has the same properties as the particle ($E_1 = E_2$ and $v_1 = v_2$), the maximum contact force, according to Zukas (1982), can be determined by utilizing the following equation:

$$P_{max} = \frac{4R_2^{\frac{1}{5}}(\frac{15}{16}\pi m_2 v_0^2)^{\frac{3}{5}}}{3\pi(\frac{1-v_1^2}{\pi E_1} + \frac{1-v_2^2}{\pi E_2})^{\frac{2}{5}}} \qquad (3.6)$$

For the given data such as: $v_0 = 3$ cm/s, $m_2 = 0.11$ kg, $v = 0.3$ and $E = 42194$ kg/cm^2, the maximum contact force was calculated to be:

$$P_{max} = 1.43 \text{ kg}.$$

The calculated contact force is very small and it is impossible to break the particle. However, this force is acting on the asperities of the surface. Hence, real contact area is only a few microns, so that it can be regarded as a point contact. Because contact area is much smaller than the size of the particle, the entire particle can be regarded as an infinite body in comparison with a few microns. According to Timoshenko and Goodier (1951), it can be assumed that this load creates simple radial

stress near the contact point in the coal particle. Then the magnitude of radial stress near the contact point can be determined. As shown in Figure 3.26, the radial stress increases exponentially with the decrease in the distance to the contact point. Under the influence of a compressive load of 1 kg, local stress within the 10 micron range, around the contact point, is as high as $1x10^4 \sim 1x10^5$ kg/cm^2. This local stress is high enough to break the asperities. Therefore, it can be concluded that any contact action will generate dust no matter how slight the contact action is.
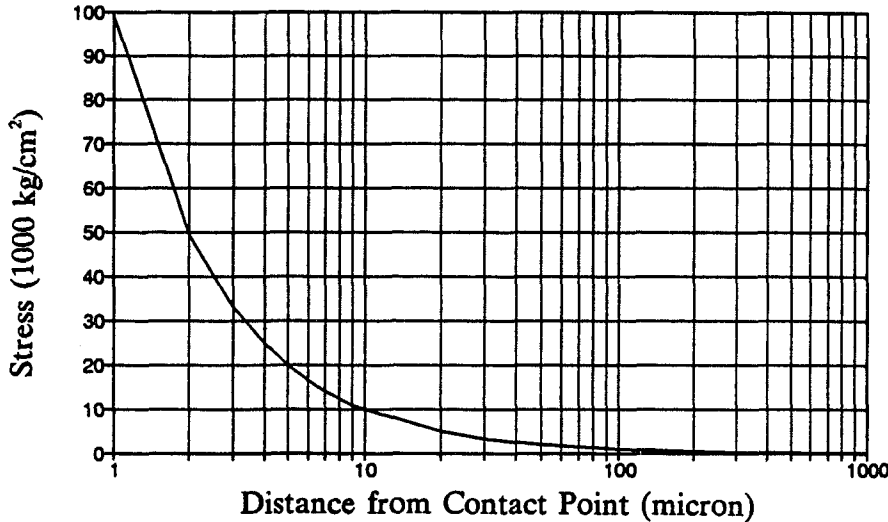
Figure 3.26. The magnitude of stress near the finite contact point
under a contact force of 1 kg

Because the asperities on coal surface are at various levels, when the higher level asperities fail lower asperities will take part in contact successively. The contact

area increases with the increase in the number of contact points. Thus, the contact reaches stable state.

Sliding and Rolling Attrition

When a coal particle slides or rolls on the surface of another coal particle or other objects, a surface layer is removed from the particle. Though this layer is extremely thin, usually a few microns, it makes significant contribution to airborne dust generation. This point can be proven by sliding a coal particle on a sheet of white paper. As a result, it produces a black trace on the surface of the paper even if no additional normal pressure is applied. The process of sliding attrition consists of two stages. The first stage is formation of contact points, where asperities of both surfaces penetrate each other and form an engagement as shown in Figure 3.27. The second stage is rupture of asperities, where the asperities are ruptured by the excessive shear stress of driving force.
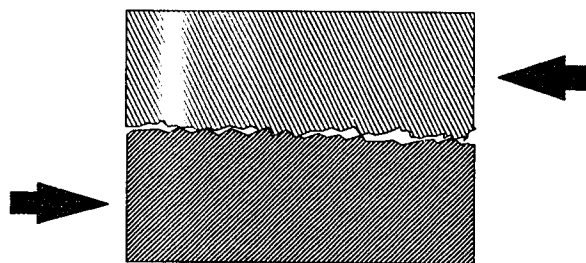
Figure 3.27. Illustration of surface engagement and sliding attrition

The amount of dust generated due to sliding is directly proportional to the weight loss of particles. The amount of weight loss depends on a number of parameters, such as distance of sliding, the properties of coal materials, surface characteristics of coal particles and the other objects on whose surface the sliding takes place.

Combined Attrition

In practice, coal particles are subject to combined action of contacting, sliding and rolling. To study the generation of dust and fine particles due to the combined action, an assemblage of coal particles with a certain size range were loaded in a rotating drum. The drum had a diameter of 14 cm and a length of 11 cm , and was constructed of brass, comprising a 2 mm standard mesh, as shown in Figure 3.28. When the drum rotated, the coal particles in the drum slid or rolled on the wall of the drum, impacted the bottom of the drum, and contacted one another. Dust and fine particles were generated by the combination of the actions mentioned above. With 350 grams of coal particles in the drum, Figure 3.29 shows dust and fine particles generated after running the drum for 1 minute at 20 rpm. The particle size used in the experiment was in the range of 3.18~3.81 cm. The result indicates that though the impact and sliding was very slight, the amount of dust and fine particles generated was significant.
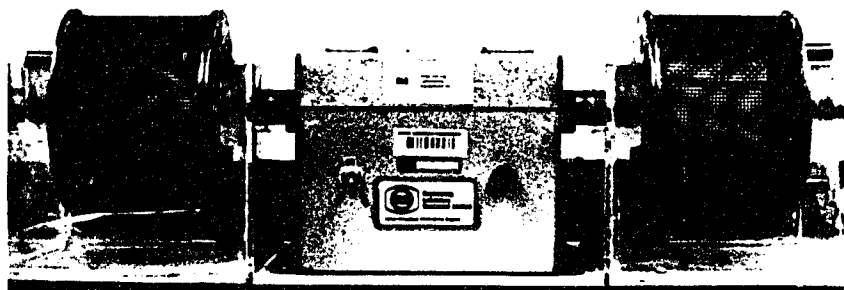
Figure 3.28. Apparatus for attrition experiments
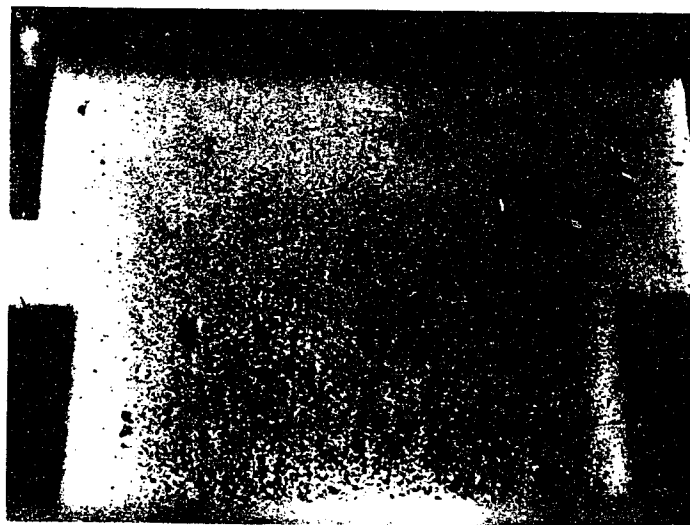
Figure 3.29. Dust and fine particles generated by 350 grams of coal
particles subjected to a slight attrition for 1 minute

To study the effect of operating time, particle size and coal properties on the amount of dust and fine particles produced due to attrition, the experiment was conducted for 15 minutes. The weight loss was measured every minute. The results are shown in Figure 3.30. It indicates that the amount of weight loss of coal particles, caused by attrition, is directly proportional to the operating time. Figure 3.30 also shows that the amount of weight loss increases as the particle size decreases. This is due to the fact that small particles have a greater total surface area per unit weight of material and possess a larger contact area than large particles. However, when the size of particle is smaller than 1.25 cm, contact action is very slight and the failed surface layer is much thinner. In this case, total weight loss is less, as shown in Figure 3.31. Though the total weight loss is less, a larger fraction of airborne dust in the weight loss could be expected because of thinner failure layers. The effect of coal properties on the amount of dust and fine particles generated due to attrition is shown in Figure 3.32. Lower Kittanning coal has a higher grindability index, a higher abrasivity index, and lower strength. It yielded a larger amount of dust and fine particles than Waynesburg coal.
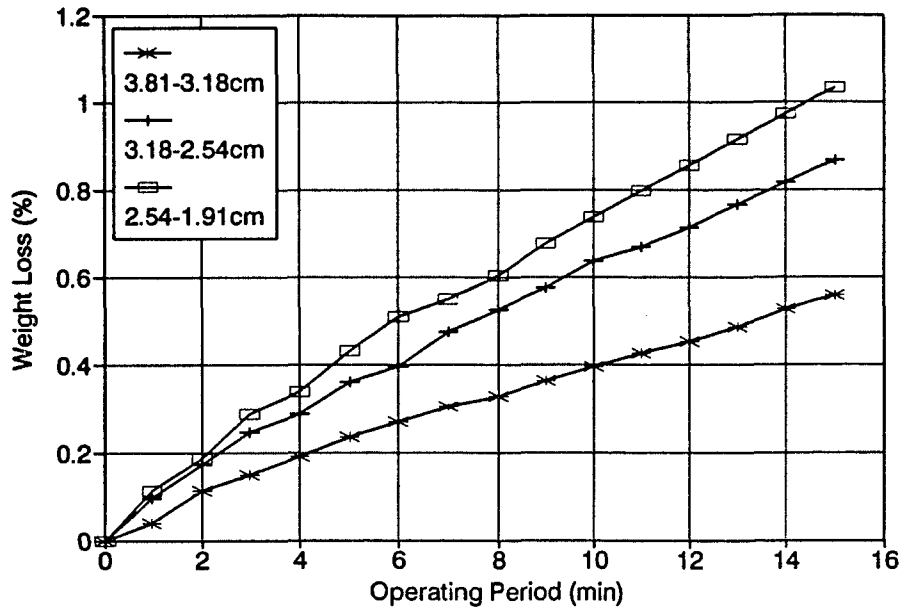
Figure 3.30. Particle weight loss due to combined attrition and size effect
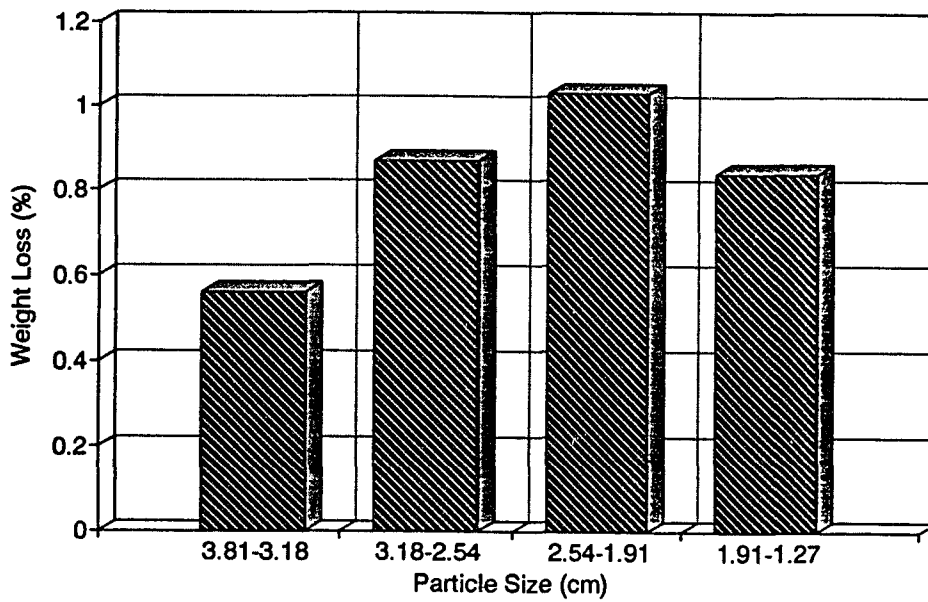
Figure 3.31. Effect of particle size on weight loss due to attrition

61
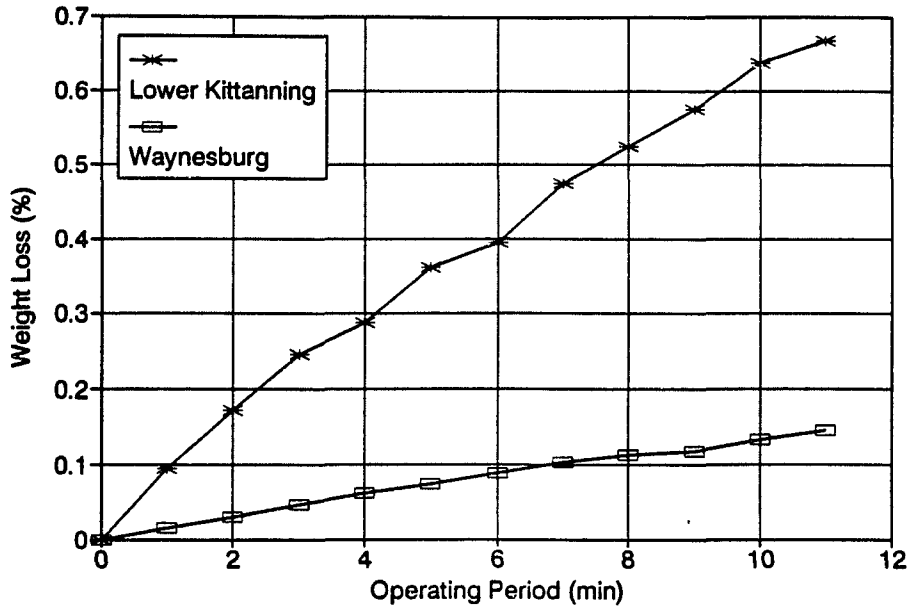
Figure 3.32. Effect of coal property on weight loss
of coal particles due to attrition

Chapter 4
MATHEMATICAL MODELING OF REGRINDING PROCESS

In order to study the principles of the regrinding process and the resulting

dust generation, it is important to understand the mechanisms of breakage of

particles. However, since the feed is always an assemblage of particles, single

particle breakage analysis is not sufficient for predicting the outcome of regrinding

and evaluating the amount of dust generation during the process. It is noted that

regrinding is a process whereby feed becomes product and both feed and product

contain a wide range of particle sizes. In order to predict the results of regrinding

and evaluate the amount of dust generation, it is necessary to study the relationship

between feed and product in whole range of particle sizes.

Feed Size Distribution

The feed consists of coarse material which is mined from primary cutting. It

contains a wide range of particle sizes and can be presented by a size distribution

model, either in frequency form or cumulative form. Figure 4.1 shows a size

distribution of coal particles by mass, produced in a small scale primary coal cutting

(Khair 1984). As Khair pointed out, size distribution of coal particles in primary

63

cutting varied with three groups of parameters, namely, operating parameters, in-situ stress in coal seam and coal properties. Because of the complexity and uncertainty of size distribution, instead of choosing simple or complex mathematical function to express the plot of feed size distribution, a vector distribution model is used. Assuming that the feed has a size distribution as shown in Figure 4.2, then a feed list, namely, f_1, f_2, f_3, ..., f_m, can be obtained from Equation (4.1):

$$f_j = w_j W \qquad (4.1)$$

where f_j represents the mass of particles of size range j, w_j is per cent mass of the particles of size range j and W is the mass of total feed material. As a result, the feed list forms a vector $\{f_1, f_2, f_3, ..., f_m\}$ and is denoted by vector $\{F\}$.
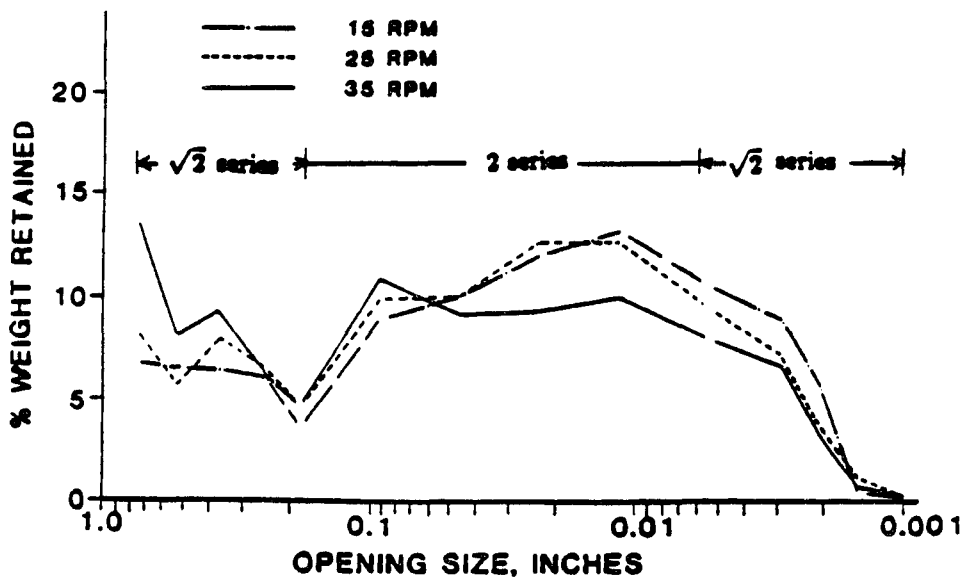
Figure 4.1. Typical size distribution of coal particles from a small scale primary cutting, (1 inch = 2.54 cm) (after Khair, 1984)
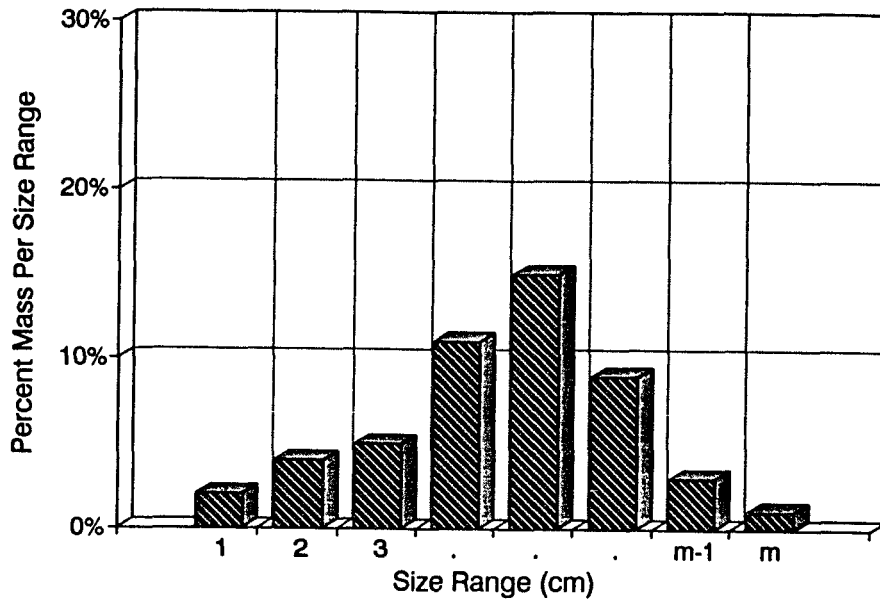
Figure 4.2. Plot of feed size distribution by mass
in frequency form

Probability of Breakage and Select Function

When feed particles are subjected to the regrinding process, every particle

may break in three possible mechanisms as discussed before. There is uncertainty

in the breakage of particles. Assuming that for a particle in size range j, the

breakage probability of the particle is s_j. Then, the rate of breakage for the feed

particles f_j is $s_j f_j$, where s_j is known as specific rate of breakage or select function.

The select function depends on the size of feed particles. In other words, one size

range has different select function from another. Therefore, select functions for

whole range of feed particle sizes compose a selection vector {S}. It can also be

written in diagonal matrix, known as select matrix as expressed in Equation (4.2):

$$[S] = \{s_1, s_2, \ldots, s_m\}$$

$$\text{or} \quad [S] = \begin{bmatrix} s_{11} & 0 & 0 & 0 \\ 0 & s_{22} & 0 & 0 \\ \cdots & \cdots & \cdots & \cdots \\ 0 & 0 & 0 & s_{mm} \end{bmatrix} \tag{4.2}$$

Generally speaking, select function for small particles is less than that for large particles because more discontinuities or weak planes may be involved in the larger particles and weaken the strength of the particles. To show the effect of particle size on select functions, particles of different sizes were selected from the Lower Kittanning coal seam. The particles were sized into four size ranges. For each size range, about 50 irregularly shaped coal particles were dropped to impact a concrete floor at a velocity of 4.17 m/s. The select function for each particle size range was calculated by taking the ratio of the number of broken particles to the number of total particles. The result is given in Figure 4.3. It indicates that select function increases with particle size. The select function for particles of the size range of 1.91~2.54 cm is about two times as much as that for particles of the size range of 1.25~1.91 cm.

66
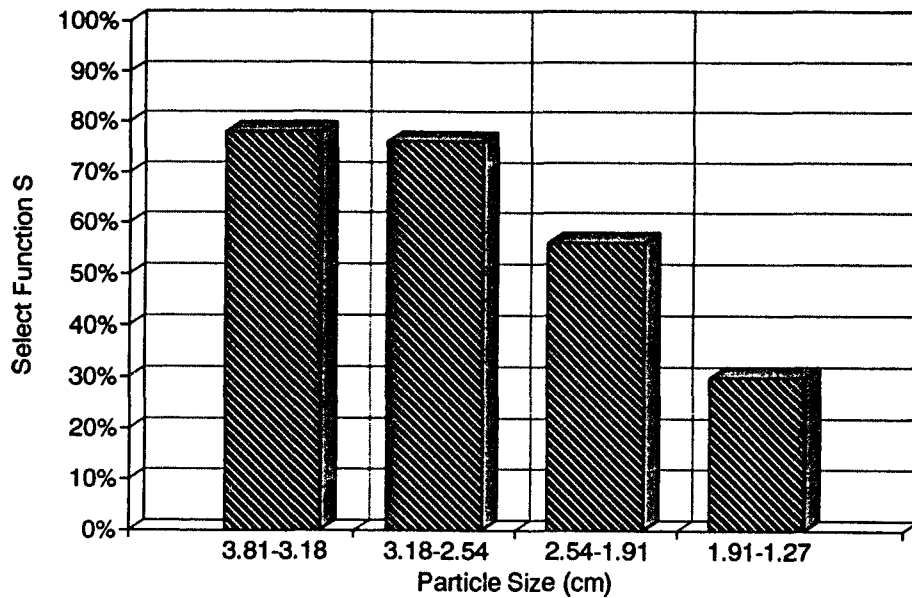
Figure 4.3. Effect of particle size on select function

In addition to particle size, a number of other parameters could also affect the select function. They are discussed as follows:

Cutting Velocity

Cutting velocities determine the amount of kinetic energy transferred to coal particles from the cutting head. A higher cutting velocity makes coal particles gain a higher impact velocity and store more strain energy during impact action, hence increasing the probability of breakage. Utilizing Lower Kittanning coal particles to impact concrete floor, the effect of initial impact velocity on select functions was

investigated. The results are shown in Figure 4.4. It indicates that select function increases with impact velocity rapidly.
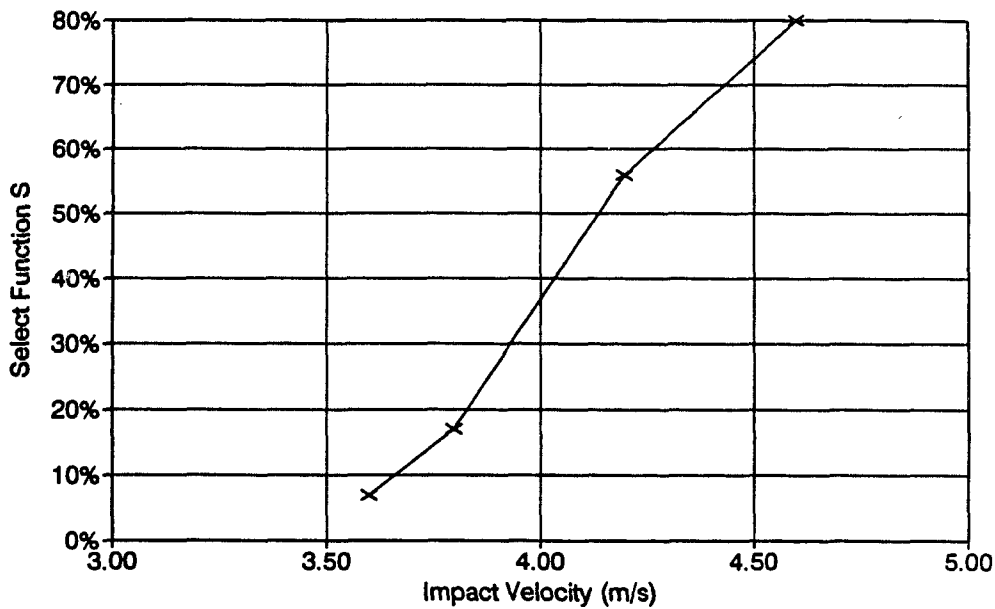
Figure 4.4. Effect of impact velocity on select function

Duration of Regrinding

The duration of regrinding influences the regrinding outcome in many ways: A longer regrinding period increases the number of impact events, hence increasing the probability of breakage. Furthermore, successive impact events could affect select function cumulatively. A particle is weakened in an impact event even

68

though it does not break, and it increases the probability of breakage in the succeeding impact event. In this case selection function will increase with the duration of regrinding in an increasing rate. In order to investigate the effect of successive impact events on the breakage of particles, irregularly shaped Lower Kittanning coal particles were utilized to impact a concrete floor at a velocity of 4.17 m/s. The number of broken particles in the first impact event was counted. The select function for the first impact event was calculated by taking the ratio of the number of the broken particles to the number of utilized particles. The unbroken particles were subjected to second impact event at the same velocity. The select function in the second impact event was calculated by taking the ratio of the number of broken particles to the number of particles involved in the second impact event, and so on. Cumulative select functions were calculated by taking the ratio of the cumulative number of broken particles in the successive impact events to the number of particles utilized in the first impact event. The results are shown in Figure 4.5. It indicates that the select function is higher in succeeding impact event than in the preceding impact event. Cumulative select function increases with the number of successive impact events. For a machine with given parameters, the duration of regrinding mainly depends on the length of cutting path, hence depending on the depth of sump.
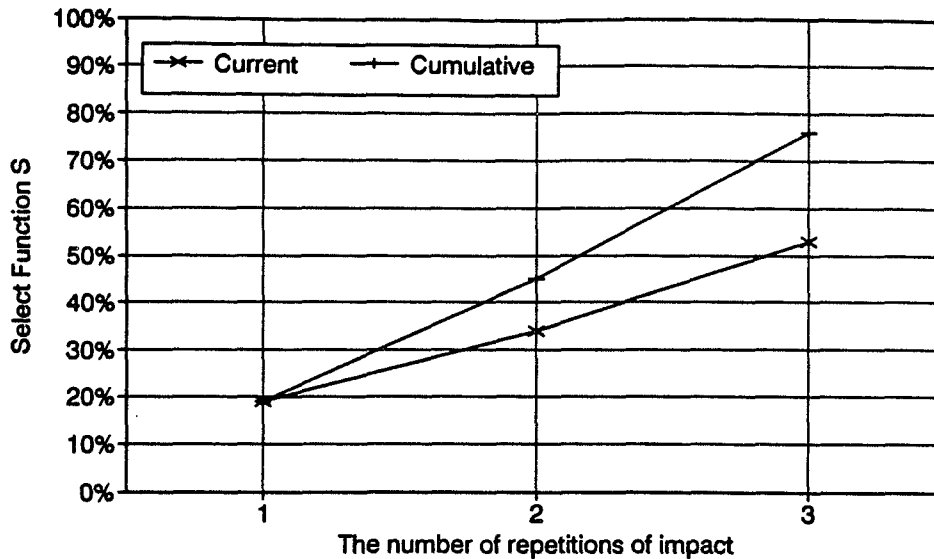
Figure 4.5. Effect of successive impact events on select function

Coal properties including mechanical properties and physical properties, such as compressive strength and tensile strength, will significantly affect select functions. Table 4.1 lists the properties and select functions of Wayensburg coal and Lower Kittanning coal. The data were obtained by utilizing irregularly shaped coal particles to impact a concrete floor at a velocity of 4.17 m/s.

Table 4.1 Effect of coal properties on select function

Type of Coal	Compressive Strength (kg/cm^2)	Tensile Strength (kg/cm^2)	Select Function $(\%)$
Waynesburg	519.5	10.3	42
Lower Kittanning	191.5	6.3	70

Product Size Distribution and Breakage Distribution Function

The breakage of any selected particles produces a suite of daughter particles which have a size smaller than the mother particles. This suite has its own size distribution in a vector form, expressed as $p_{i,j}$, (where i=1, 2, ..., n represents product particle size range and subscription j represents feed particle size range from which the product are obtained). Let $b_{i,j} = p_{i,j}/s_j f_j$, where $b_{i,j}$ is known as breakage distribution function which is determined by size distribution characteristics. Breakage distribution function depends on a number of factors. First, it depends on feed particle size. For a given small size range, breakage distribution function composes a vector. For whole range of feed particle sizes, the breakage distribution function is a matrix, known as breakage distribution matrix as expressed in Equation (4.3):

$$[B] = \begin{bmatrix} b_{11} & b_{12} & \cdots & b_{1m} \\ b_{21} & b_{22} & \cdots & b_{2m} \\ \cdots & \cdots & \cdots & \cdots \\ b_{n1} & b_{n2} & \cdots & b_{nm} \end{bmatrix} \qquad (4.3)$$

Second, the breakage distribution function depends on coal properties, such as texture, size and distribution of cleats, and the strength of coal materials. For example, the properties of Waynesburg coal and Lower Kittanning coal were significantly different and they yielded completely different sizes of product when

71

subjected to impact on a concrete floor, as shown in Figure 4.6.
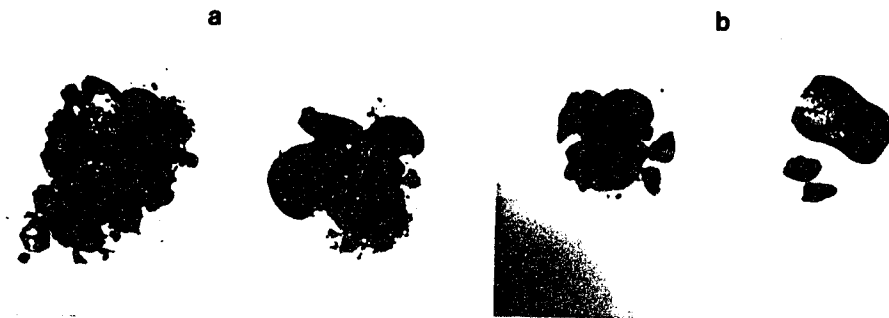
Figure 4.6. Effect of coal properties on impact product
a-Lower Kittanning coal, b-Waynesburg coal

The velocity of cutting head, which determines the impact velocity, also has

a significant effect on breakage distribution functions. Figure 4.7 shows products of

Lower Kittanning coal particles resulted from different impact velocities.
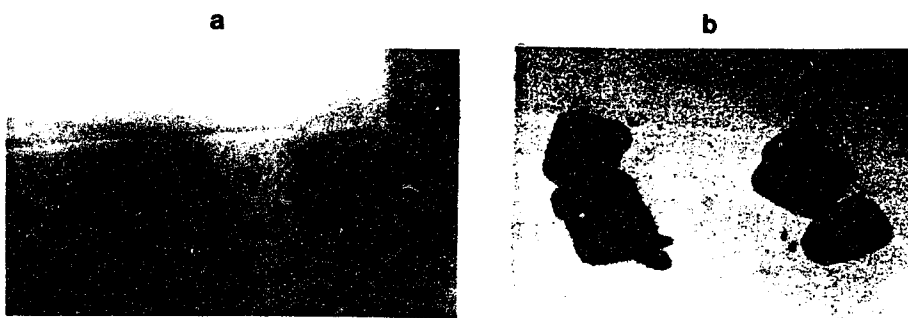
Figure 4.7. Effect of impact velocity on impact product
a - v=4.32 m/s, b - v=4.70 m/s

72

The Relationship Between Feed and Product

When a wide range of particle sizes are fed into a system, the amount of

broken particles, W_b, can be determined by Equation (4.4):

$$W_b = \sum_{j=1}^{n} s_j \, f_j \qquad (4.4)$$

The amount of unbroken particles, W_r, will be determined by Equation (4.5):

$$W_r = \sum_{j=1}^{n} (1-s_j) f_j \qquad (4.5)$$

Total product, P_t, is the sum of broken particles and unbroken particles, as

expressed in Equation (4.6):

$$P_t = \sum_{j=1}^{n} s_j \, f_j + \sum_{j=1}^{n} (1-s_j) \, f_j \qquad (4.6)$$

And the relationship between product size distribution and feed size

distribution can be expressed as Equation (4.7):

$$\{P\}= [B] * [S] * \{F\} + ([I]-[S]) * \{F\} \qquad (4.7)$$

where $\{P\} = \{p_1, p_2, \dots, p_n\}^T$, the product size distribution,

$\{F\} = \{f_1, f_2, \dots, f_n\}^T$, the feed size distribution,

$[B] = b_{ij}$, (i=1,2,3,...,n and j=1,2,...,m), the breakage distribution matrix,

$[S] = s_{ij}$, (i=1,2,3,...,n; j=1,2,3,...m), the select matrix, $s_{ij} = 0$ when $i \neq j$,

$[I]$ is a unit matrix.

Let [C] = [B][S] + [I]-[S]. A simple equation can be obtained such as:

$$\{P\} = [C] * \{F\} \tag{4.8}$$

where [C] is known as correlation matrix of size distributions.

Table 4.2 further explains how the feed becomes the product. Assuming that f_j (j=1,2,3,...,m) yields a column product $p_{i,j}=b_{i,j}s_jf_j$, (i=1,2,...,n). For a given product particle size range i, the amount of product p_i is the sum of the products in the specified row from each feed. Then, overall product size distribution can be obtained as shown in Table 4.2.

Table 4.2 Relationship between feed and product

Overall Product	Product from each feed size				
	f_1	f_2	...	f_{m-1}	f_m
p_1	$(1-s_1)f_1$	0		0	0
p_2	$b_{2,1}s_1f_1$	$(1-s_2)f_2$		0	0
p_3	$b_{3,1}s_1f_1$	$b_{3,2}s_2f_2$		0	0
...	...	...	...	...	...
p_{n-1}	$b_{n-1,1}s_1f_1$	$b_{n-1,2}s_2f_2$		$b_{n-1,m-1}s_{m-1}f_{m-1}$	$b_{n-1,m}s_mf_m$
p_n	$b_{n,1}s_1f_1$	$b_{n,2}s_2f_2$		$b_{n,m-1}s_{m-1}f_{m-1}$	$b_{n,m}s_mf_m$

In Equation (4.8), product size distribution vector {P} includes all products from large particles to dust particles. Theoretically speaking, the amount of dust can be determined from the equation if [C] and {F} are given. However, the amount of dust is little in comparison with the total product so that it can be

74

neglected when overall product size distribution is concerned. In order to evaluate the amount of dust product accurately, dust product needs to be calculated separately. Since dust concentration in the air is of most important, a mathematical formulation for the dust concentration caused by regrinding is given in Equation (4.9):

$$D = \{ C_d \}\{ F \} \qquad (4.9)$$

where D is dust concentration, $\{C_d\} = \{c_{d1}, c_{d2}, ..., c_{dm}\}$ is dust concentration coefficient vector. Dust concentration coefficient c_{dj} represents the dust concentration resulted from regrinding a unit weight of coal particles of size range j. The unit of dust concentration coefficient is $mg/m^3/kg$.

The size distribution of dust mass, D, can also be related to feed size distribution as expressed in Equation (4.10):

$$\begin{Bmatrix} d_1 \\ d_2 \\ \cdot \\ \cdot \\ \cdot \\ d_k \end{Bmatrix} = \begin{bmatrix} c_{d11} & c_{d12} & \cdots & c_{d1m} \\ c_{d21} & c_{d22} & \cdots & c_{d2m} \\ \cdots & & \cdots & \\ c_{dk1} & c_{dk2} & \cdots & c_{dkm} \end{bmatrix} \begin{Bmatrix} f_1 \\ f_2 \\ \cdot \\ \cdot \\ \cdot \\ f_m \end{Bmatrix} \qquad (4.10)$$

The feed size distribution is derived by primary cutting conditions. With the model presented above, the product and dust concentration could be evaluated if

75

[C] and $\{C_d\}$ are determined. [C] and $\{C_d\}$ depend on select functions and breakage distribution functions. Therefore [C] and $\{C_d\}$ may be estimated through evaluating [S] and [B]. However, quantitatively evaluating [S] and [B] is very difficult since they depend on a number of factors, including random factors. In practice, correlation matrix [C] and dust concentration coefficient vector $\{C_d\}$ can be determined through experimental investigations.

Chapter 5
LABORATORY SIMULATION OF REGRINDING PROCESS

The result of regrinding and the amount of dust generation are machine operating parameter and field condition dependent. This indicates that the best and reliable approach to evaluate the product and the amount of dust generated due to regrinding is field investigation. However, in the field, the product is a combined result of primary cutting and regrinding action. The dust concentration that can be obtained is also caused by both primary cutting and regrinding. There is no way to separate regrinding effect from primary cutting effect in the field. In addition, dust also comes from some other sources such as roof caving, loading and transportation. This complicated situation makes it impossible to evaluate dust generation due to regrinding in the field. A laboratory simulation is an appropriate means to evaluate dust generation due to regrinding and to determine dust concentration coefficients expressed in Equation (4.9). Although it is impossible to exactly simulate the field condition in the laboratory, the results revealed in the laboratory can be meaningful and could be used as guidance in the field.

Automated Rotary Coal Cutting Simulator

The Automated Rotary Coal Cutting Simulator (ARCCS) was originally designed with the capability to study different machines and in-situ parameters that influence fragmentation of coal and resulting dust generation. It consists of a main frame, a confining chamber, a rotary cutting drum, bit blocks, a hydraulic power supply and a control unit. In order to meet the need of the simulation of the regrinding process, the ARCCS was modified with: 1) A cowl to hold a coal block at the bottom of the confining chamber. This cowl has built in hydraulic cylinders to advance the coal block upwards to simulate the downward movement of the cutting head; 2) A hopper-like feeder to be used in feeding the predetermined size and amount of coal particles on to the entire width of the cutting drum to simulate the mined coal from primary cutting; 3) An enclosure to completely cover up the cutting head which enables the investigator to collect airborne dust. The space of the enclosure was about 0.45 m³. Figure 5.1 shows modified ARCCS.

The chamber can house a coal block of approximately 38 cm wide, 48 cm high and 20 cm thick. The cutting head is 48 cm in diameter which can house 22 bits. The maximum revolutions per minute (rpm) of the cutting head is 45~50. Advancing rate, rpm, and the rate of feed can be controlled for experimental purposes.
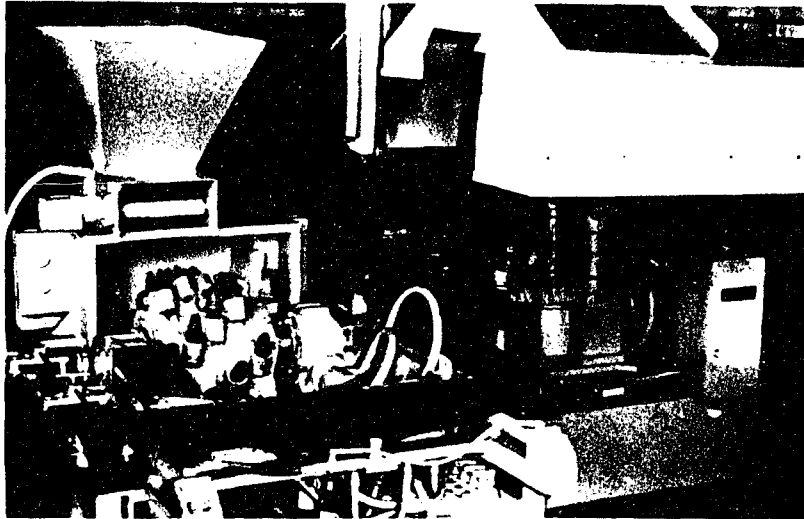
Figure 5.1. Modified ARCCS

Simulation of Regrinding Process

To utilize the Automated Rotary Coal Cutting Simulator to simulate a regrinding process, coal blocks were set up in the front and at the bottom of the cutting head to simulate intact coal seam. The blocks were cut by advancing the cutting head to create a circular cutting path. When the predetermined depth of sump or length of cutting path was obtained, the cutting head stopped advancing and coal product from primary cutting was cleaned. Then, coal particles were fed into the cutting path while the cutting head kept rotating without advancing. Thus, product and dust resulted from regrinding could be separated from primary cutting.

79

In order to establish the relationship between product size distribution and feed size distribution in a matrix form as expressed in Equation (4.8) and determine dust concentration coefficients in Equation (4.9), particles of different size ranges were fed separately. In this study, four size ranges were utilized. The size ranges were specified as follows:

size range I: 3.81~3.18 cm,

size range II: 3.18~2.54 cm,

size range III: 2.54~1.91 cm,

size range IV: 1.91~1.27 cm.

Products were collected and dust samples were taken for each feed.

Experimental Procedure

In order to conduct laboratory simulation of the regrinding process as described above, the following experimental procedure was carried out.

Coal Specimen Preparation

Waynesburg coal fragments were obtained from the field. Utilizing screen sieving in the laboratory, the coal fragments then were sized to obtained particles of specified sizes, such as size range I, II, III, and IV.

Large coal blocks were also prepared from Waynesburg coal seam. The coal

blocks were cut into the following two sizes: 18cm x 33cm x 43cm blocks to be set up in the confining chamber in front of the cutting head, and 15cm x 18cm x 33cm blocks to be placed underneath the cutting head.

The blocks were molded with plaster of Paris in order to obtain perfect dimensions.

Dust Sampler Preparation

Marple personal cascade impactors, Series 296, were used to measure dust concentration. These impactors have six stages and a backup filter. They can give complete, accurate aerodynamic particle size distributions. As shown in Figure 5.2, the principle of sampling is that the flow enters the inlet cowl and accelerates through the six radial slots in the first stage of impactors. Particles larger than the cut point of the first stage impact on the perforated collection substrate. Then, the air-stream flows through the narrower slots in the second stage of impactors, smaller particles impact on the second collection substrate and so on. The width of the radial slots are constant for each stage but are smaller for each succeeding stage. Thus, the jet velocity is higher for each succeeding stage, and smaller particles eventually acquire sufficient momentum to impact on one of the collection substrates.

Cascade impactors were prepared 24 hours before they were used. The preparation included cleaning each of the stages and the cowl, evenly spraying grease

on each substrate to form a grease film under the slots of the preceding stage. The original weight of the substrate was measured immediately before an experiment was conducted.

Three cascade impactors were installed inside the enclosure, one at the bottom, one at the middle and one at the top horizons, with respect to the position of the cutting head, as shown in Figure 5.3. DU-PONT air pumps were used with cascade impactors and the air flow rate was 2 liters per minute. The air pumps were recharged to full before each experiment.
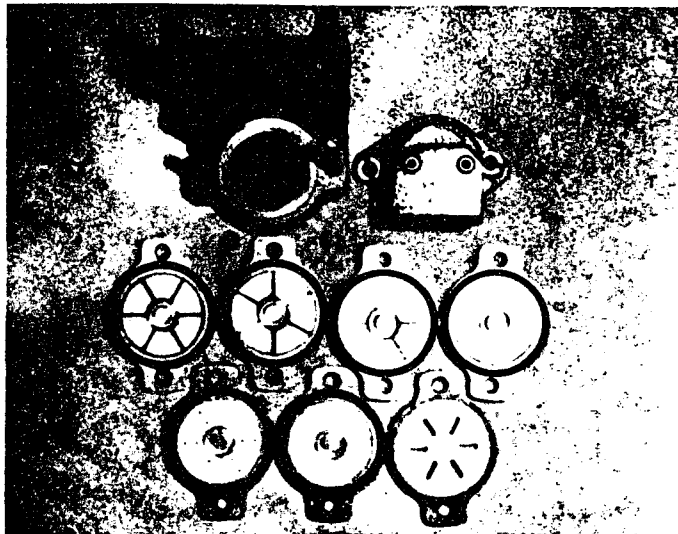
Figure 5.2. Disassembled 296 cascade impactor
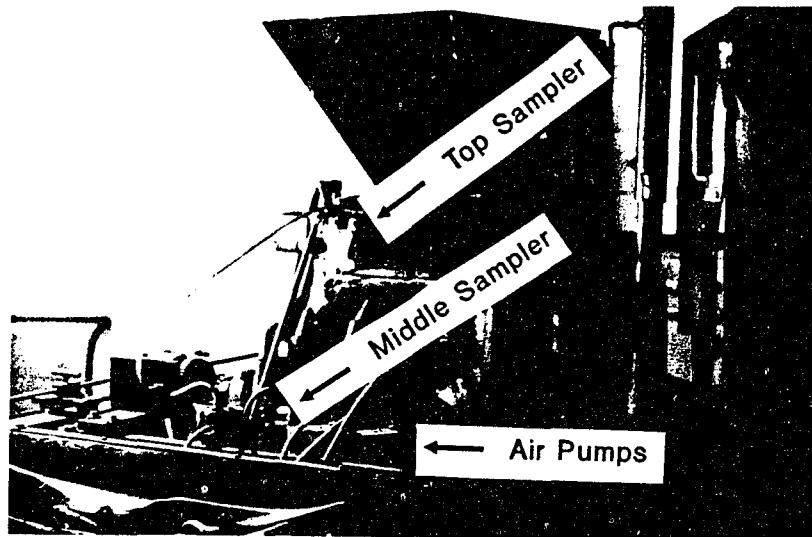
Figure 5.3. Positions of dust samplers

Experimental Operation

After all the preparations were completed, one coal block was placed in the

front chamber and another one was placed underneath the cutting head. Hydraulic

jacks were used to apply certain confining pressure to the blocks, as shown in Figure

5.4. Prior to the start of a regrinding experiment, the blocks were cut to create a

depth of sump of 5 cm. The velocity of cutting head was set to 45 rpm. Four

experiments were run by feeding f_1, f_2, f_3, and f_4 separately, where f_1, f_2, f_3, and f_4

represents the amount of feed for size range I, II, III and IV, respectively. Each

experiment lasted for three minutes. In the first two minutes, 11.3 kg of coal particles

were fed in every other 1/2 minute. In the third minute no coal particles was fed while the cutting head kept rotating. In each experiment, dust was sampled. Dust sampling lasted for three minutes and the collected weights of dust were measured. The product, including settled dust, was also collected for size distribution analysis.
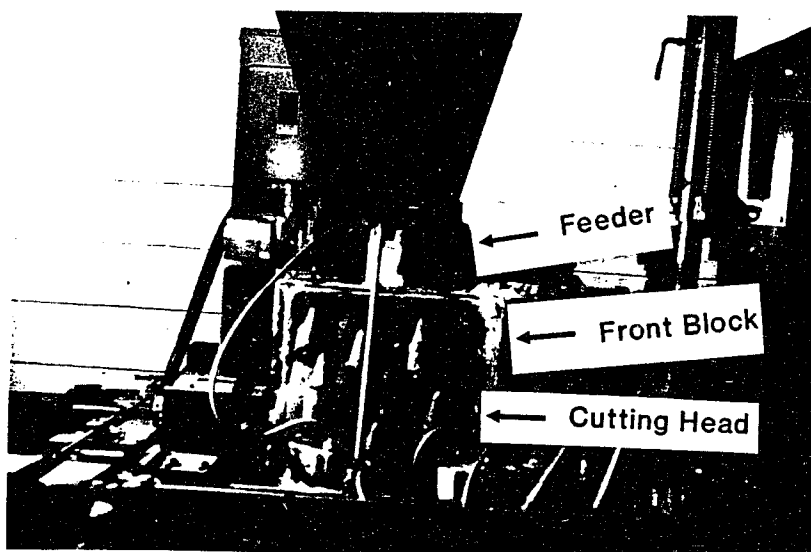
Figure 5.4. Experimental set-up

Analysis of Experimental Results and Data

Experimental results are given in Tables 5.1-4. Table 5.1 presents the products collected in the experiments. The first column of the table lists the product size ranges. The second column lists the size distribution of total product from four feeds. The rest of the columns lists the size distribution of product from each feed.

Table 5.2 presents the amount of dust collected on each stage of the top cascade impactor. Table 5.3 lists the amount of dust collected on each stage of the middle cascade impactor and Table 5.4 lists the average values of the top and the middle cascade impactors. The first columns of the tables list the geometric mean diameter (GMD) of dust particles. The second columns list the amount of total dust on the same stages from four feeds. The rest of the columns list the amount of dust collected on each stage for a specified feed.

Table 5.1 Size distribution of product

Product size range	Product (kg)				
	Total	from f_1	from f_2	from f_3	from f_4
p_1 (3.81~3.18 cm)	20.11	20.11	0.00	0.00	0.00
p_2 (3.18~2.54 cm)	22.49	1.63	20.86	0.00	0.00
p_3 (2.54~1.91 cm)	21.90	0.29	0.91	20.70	0.00
p_4 (1.91~1.25 cm)	22.63	0.09	0.23	0.86	21.45
p_5 (<1.25 cm)	3.53	0.52	0.68	1.11	1.22

Table 5.2 Dust collected on each stage of the top impactor

GMD (micron)	The amount of dust (mg)				
	Total	from f₁	from f₂	from f₃	from f₄
12.25	6.37	0.84	1.59	1.84	2.10
7.75	1.72	0.23	0.28	0.44	0.77
4.58	1.04	0.19	0.12	0.25	0.48
2.65	0.12	0.01	0.04	0.03	0.04
1.34	0.04	0	0.01	0.01	0.02
0.67	0	0	0	0	0
<0.67	0	0	0	0	0
Total	9.29	1.27	2.04	2.57	3.41

GMD - Geometric Mean Diameter
Sampling period 3.0 minutes, the rate of air flow 2 liters per minute.

Table 5.3 Dust collected on each stage of the middle impactor

GMD (micron)	The amount of dust (mg)				
	Total	from f₁	from f₂	from f₃	from f₄
12.25	10.3	1.75	2.33	2.66	3.29
7.75	4.18	0.35	0.64	0.76	2.43
4.58	1.52	0.08	0.14	0.42	0.88
2.65	0.21	0.03	0.05	0.07	0.06
1.34	0.07	0.01	0.01	0.01	0.04
0.67	0.01	0.00	0.00	0.00	0.01
<0.67	0.00	0.00	0.00	0.00	0.00
Total	16.02	2.22	3.17	3.92	6.71

Table 5.4 Dust collected on each stage
(average of the top and the middle impactors)

GMD (micron)	The amount of dust (mg)				
	Total	from f_1	from f_2	from f_3	from f_4
12.25	8.20	1.30	1.96	2.25	2.70
7.75	2.95	0.29	0.46	0.60	1.60
4.58	1.28	0.14	0.13	0.34	0.68
2.65	0.17	0.02	0.05	0.05	0.05
1.34	0.06	0.01	0.01	0.01	0.03
0.67	0.01	0.00	0.00	0.00	0.01
<0.67	0.00	0.00	0.00	0.00	0.00
Total	12.67	1.75	2.61	3.25	5.06

From the data presented in Table 5.1, a typical relationship between product size distribution and feed size distribution was obtained as expressed in Equation (5.1).

$$\begin{Bmatrix} p_1 \\ p_2 \\ p_3 \\ p_4 \\ p_5 \end{Bmatrix} = \begin{bmatrix} 0.877 & 0 & 0 & 0 \\ 0.072 & 0.920 & 0 & 0 \\ 0.013 & 0.040 & 0.913 & 0 \\ 0.004 & 0.010 & 0.038 & 0.946 \\ 0.023 & 0.030 & 0.049 & 0.054 \end{bmatrix} \begin{Bmatrix} f_1 \\ f_2 \\ f_3 \\ f_4 \end{Bmatrix} \qquad (5.1)$$

Both feed size distribution and production size distribution are plotted in Figure 5.5. It indicates that there is no significant difference between product size distribution and feed size distribution. This is due to the fact that because of low velocity of the cutting head, only a few particles were subjected to breakage.
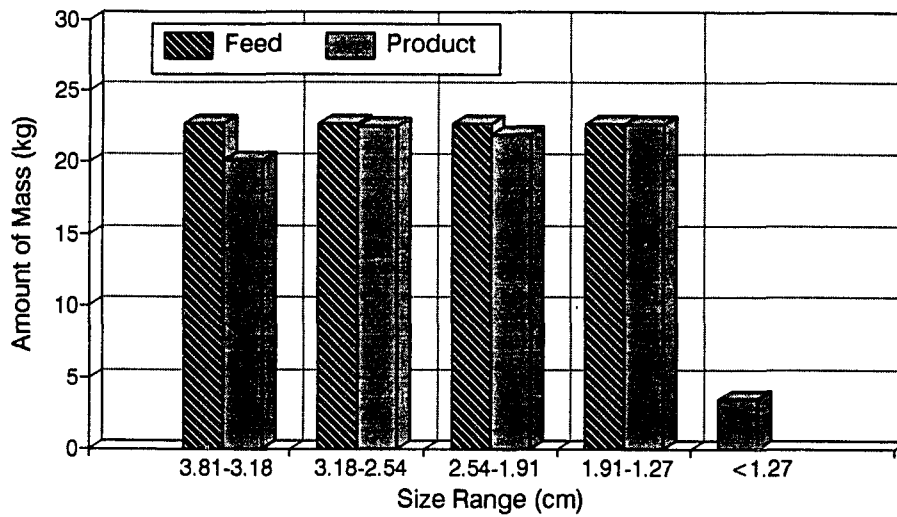
Figure 5.5. Feed size distribution and product size distribution chart

Since only a few particles were subjected to breakage, select functions were very small. Equation (5.2) expresses the select matrix obtained from the experimental results.

$$[S] = \begin{bmatrix} 0.113 & 0 & 0 & 0 \\ 0 & 0.080 & 0 & 0 \\ 0 & 0 & 0.087 & 0 \\ 0 & 0 & 0 & 0.054 \end{bmatrix} \qquad (5.2)$$

88

The select matrix indicates that select function varies with particle size. Basically, the select function increases with particle size, as shown in Figure 5.6.
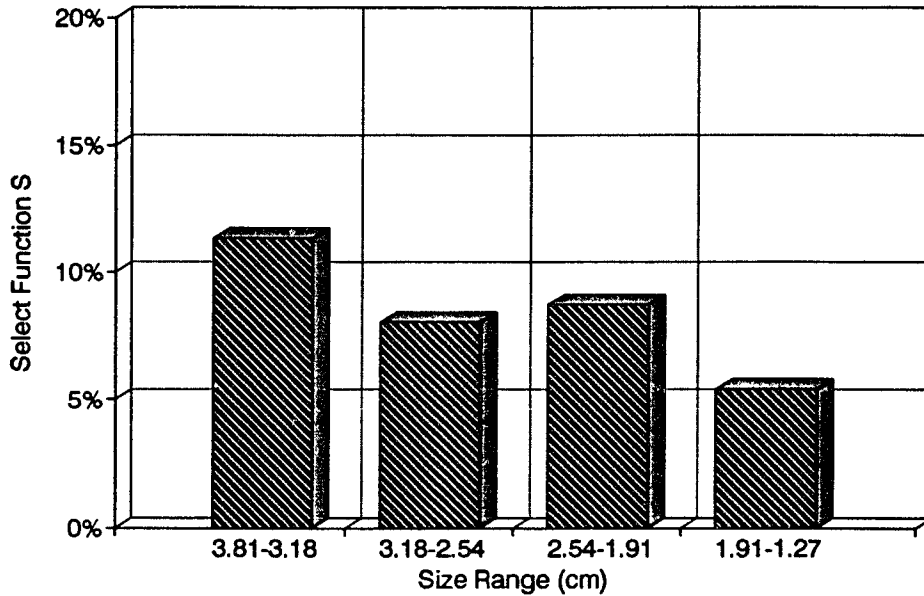
Figure 5.6. Relationship between select function and feed particle size

Utilizing the average values of the top and middle dust samplers presented in Table 5.4, a relationship between size distribution of sampled dust and feed size distribution was obtained as expressed in Equation (5.3). The total dust concentration produced by four feeds is presented in Equation (5.4). The relationship between dust concentration coefficients and particle sizes is shown in Figure 5.7. The results indicate that dust concentration coefficient increases as feed particle size decreases. Regrinding of small particles produces more dust.

$$\begin{Bmatrix} d_{12.25} \\ d_{7.75} \\ d_{4.58} \\ d_{2.65} \\ d_{1.34} \end{Bmatrix} = \begin{bmatrix} 9.56 & 14.41 & 16.54 & 19.85 \\ 2.13 & 3.38 & 4.41 & 11.70 \\ 1.03 & 0.95 & 2.50 & 4.99 \\ 0.15 & 0.37 & 0.37 & 0.37 \\ 0.07 & 0.07 & 0.07 & 0.22 \end{bmatrix} \begin{Bmatrix} f_1 \\ f_2 \\ f_3 \\ f_4 \end{Bmatrix} \qquad (5.3)$$

where the subscript i of d_i represents GMD, the unit of feed is kg and the unit of dust

concentration is mg/m^3.

$$D = \{12.94 \quad 19.18 \quad 23.89 \quad 36.63\} \{f_1 \quad f_2 \quad f_3 \quad f_4\}^T \qquad (5.4)$$

where the unit of dust concentration is mg/m^3, the unit of feed is kg and the unit of

dust concentration coefficient is $mg/m^3/kg$.
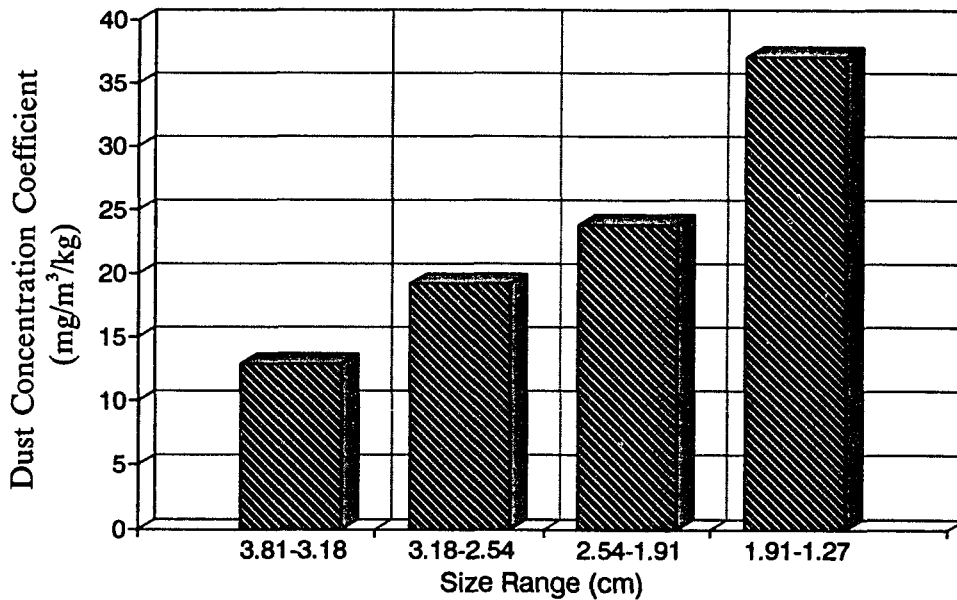
Figure 5.7. Relationship between dust concentration coefficient
and particle size

In spite of small select functions, the amount of dust generated was significant. Regrinding one kilograms of Waynesburg coal particles produces a 12.9~36.6 mg/m^3 dust concentration in an enclosed space of 0.45 m^3. It requires 3.0~8.25 m^3 air to dilute this dust concentration to an acceptable dust concentration level. In underground coal mines, if a face production is 2 tons/min and all mined coal is subjected to regrinding, it may require 6000~16500 m^3/min additional air to the face for diluting the dust or require other dust control techniques.

The experimental results show that only 5%~11% of the feed coal particles were subjected to breakage. The select function is small and it decreases as the feed particle size decreases. But the amount of dust generated due to regrinding is significant and it increases as the feed particle size decreases. This indicates that most of the dust was generated due to attrition rather than crushing.

Chapter 6
FACTORIAL EXPERIMENTAL ANALYSIS

Preliminary laboratory experiments of the regrinding process have indicated that dust generation due to regrinding was significant. However, the experiments were limited to a particular operating condition and for a given coal seam. Any change in operating conditions or change in coal seams will result in quantitative changes in product and dust generation, hence affecting dust concentration coefficients. Based on the analytical studies, the important factors influencing the regrinding process and its results for a given machine include: mechanical and physical properties of coal, depth of sump, cutting velocity or rpm of cutting head. Furthermore, the rate of feed may also affect the outcome of regrinding. Though the rate of feed does not affect the breakage of a single particle, in the cutting path, the chance for coal particles to impact one another may increase with the larger number of coal particles involved.

To estimate the effects of coal properties and operating parameters on the regrinding process and dust generation through laboratory experiment, a factorial experiment has been carried out in this study.

Factorial Experimental Design

A factorial experimental design includes selecting the levels for each parameter and constructing an experimental plan.

Influencing Parameters and Their Levels

The first step was to name each parameter or variable mentioned above, such as:

x_1 - coal properties, the type of coal or the name of coal seam,

x_2 - the depth of sump,

x_3 - the velocity of cutting head, and

x_4 - the rate of feed.

For each parameter, three levels were selected to generate a S^m symmetrical factorial, where S, the number of levels, is 3 and m, the number of factors, is 4. Codes 0, 1 and 2 were used to represent the levels, such as the first, the second and the third level, respectively. The corresponding values of each level for all parameters were selected according to the capability of the ARCCS and other available conditions, as listed in Table 6.1.

93

Table 6.1 Factors and levels

Code of level	0	1	2
Type of coal - x_1	W	P	K
Depth of sump - x_2 (cm)	5	10	15
Cutting velocity-x_3 (rpm)	25	35	45
Rate of feed x_4 (kg/min)	13.6	22.7	31.8

W-Waynesburg coal, P-Pittsburgh coal, K-Lower Kittanning coal

Three types of coal, namely Waynesburg (W), Pittsburgh (P), and Lower Kittanning coal (K), were selected to represent different properties of coal materials. Physical and mechanical properties of these coal seams were determined in the laboratory. Some important properties of these three types of coal are listed in Tables 6.2-3.

Table 6.2 Physical properties and grindability of coal seams

Type of coal	Moisture (%)	Ash (%)	Sulfur (%)	Rank	HGI	SG
W	0-1.5	13.5-13.7	2.03-2.06	HvBb*	50.43	1.42
P	0-1.1	9.7-9.8	3.44-3.48	HvAb**	60.38	1.30
K	0-1.0	8.4-8.5	0.93-0.94	HvBb	69.09	1.31

* High volatile B bituminous, ** High volatile A bituminous,
HGI-Hardgrove Grindability Index, SG-Specific Gravity.

94

Table 6.3 Mechanical properties of coal seams

Type of coal	Test orientation	σ_c (kg/cm^2)	E (kg/cm^2)	ν	σ_t (kg/cm^2)	S (kg/cm^2)
W	Face cleat	330	6186	0.33	10.8	14.3
	Butt cleat	227	8155	0.28	14.4	12.7
	Bed plane	520	3515	0.47	10.3	5.6
P	Face cleat	182	2179	0.26	8.7	6.8
	Butt cleat	198	3656	0.29	12.8	10.0
	Bed plane	280	4288	0.27	5.4	8.9
K	Face cleat	237	3726	0.22	7.7	5.6
	Butt cleat	143	4007	0.28	8.9	6.2
	Bed plane	192	2742	0.31	6.3	8.9

σ_c-compressive strength, E-Young's modulus, ν-Poisson's ratio,
σ_t-tensile strength, S-shear strength

Orthogonal Fractional Factorial Experimental Plan:

In addition to parameters and levels, some other concepts concerning a

factorial experimental design are given as follows.

Parametric combination, a parametric combination consists of one level from

each parameter.

Experimental trial, an experimental trial is referred to an experiment which is

carried out under a given parametric combination.

Experimental plan, an experimental plan contains a number of experimental

trials. Each of the trials uses different parametric combination.

For the case of four parameters and 3 levels in each parameter, the number

of all possible parametric combinations is 81. Instead of using 81 parametric

combination experimental plan, an orthogonal fractional factorial experimental plan

was employed. Dey (1985) presented a number of methods to construct an

orthogonal experimental plan for different factorials. For a S^m symmetrical

factorial, suppose S is a prime or prime power, a S^n combination experimental plan

exists, where n is determined by the equation of $m=(S^n-1)/(S-1)$. This plan can be

constructed by arranging the first n factors directly, and generating the others such

as $k_0+k_1x_1+k_2x_2+...+k_nx_n$, where k_i is an element in GF(S), and $x_1+x_2=(x_1+x_2)$ mod

S. In our case, $S=3$, $m=4$, $n=2$, $S^n=9$. Therefore, a nine parametric combination

experimental plan was constructed, as shown in Table 6.4. Trial No. or combina-

tion No., 1 to 9, were listed in the first row of the table. the level codes of x_1 and

x_2 were directly arranged in the nine combinations as shown in the table. Then,

$x_3=x_1+x_2$ and $x_4=x_1+2x_2$ were utilized to arrange level codes of x_3 and x_4 in the nine

combinations. For example, in combination No.9, $x_1=2$, $x_2=2$, $x_3=(2+2)$ mod $3=1$,

and $x_4=(2+2x2)$ mod $3=0$.

Table 6.4 Orthogonal fractional factorial experimental plan I

Trial No.	1	2	3	4	5	6	7	8	9
x_1	0	0	0	1	1	1	2	2	2
x_2	0	1	2	0	1	2	0	1	2
$x_3 = x_1+x_2$	0	1	2	1	2	0	2	0	1
$x_4 = x_1+2x_2$	0	2	1	1	0	2	2	1	0
	y_1	y_2	y_3	y_4	y_5	y_6	y_7	y_8	y_9

The plan is known as an orthogonal fractional plan because it considers only a small fraction of the complete set of parametric combinations while keeping the orthogonality that the complete set of parametric combinations possesses. The orthogonality of an experimental plan is important because it permits the estimation of all relevant effects without correlating to one another. There are two main advantages in an orthogonal fractional factorial plan. First, the experimental data are extremely simple to analyze because the level code distribution in the plan is diagonal, easily invertible. Second, the plan is optimal in a very wide sense, especially in statistical justification since it lets the investigators obtain most useful data with the least experimental work. To show these points, assume that y_1, y_2, ..., y_9 are nine results from the nine experimental trials. Utilizing the nine results, the main effects of all four parameters on dependent y can be estimated directly as shown in Table 6.5. In the table, the mean at each level for a given parameter is calculated by taking the average of those experimental results yielded from those trials whose parametric combinations contain common level code of the parameter. For example, for parameter of x_2, combinations 1, 4 and 7 contain the level 0 of x_2. Therefore, the mean at level 0 for x_2 is $(y_1+y_4+y_7)/3$.

However, the nine trial plan for 3^4 factorial is a saturated plan. It leaves no degree of freedom for error estimation. Variance analysis can not be conducted. In order to conduct statistical analysis, another 9 trial plan was constructed, as

shown in Table 6.6.

Table 6.5 Direct estimation

Factor	Means at each level	Linear effect
x_1	$A_0=(y_1+y_2+y_3)/3$ $A_1(=y_4+y_5+y_6)/3$ $A_2=(y_7+y_8+y_9)/3$	A_2-A_0
x_2	$B_0=(y_1+y_4+y_7)/3$ $B_1=(y_2+y_5+y_8)/3$ $B_2=(y_3+y_6+y_9)/3$	B_2-B_0
x_3	$C_0=(y_1+y_6+y_8)/3$ $C_1=(y_2+y_4+y_9)/3$ $C_2=(y_3+y_5+y_7)/3$	C_2-C_0
x_4	$D_0=(y_1+y_5+y_9)/3$ $D_1=(y_3+y_4+y_8)/3$ $D_2=(y_2+y_6+y_7)/3$	D_2-D_0

Table 6.6 Orthogonal fractional factorial experimental plan II

Trial No.	10	11	12	13	14	15	16	17	18
x_1	0	0	0	1	1	1	2	2	2
x_2	0	1	2	0	1	2	0	1	2
$x_3=x_1+x_2+2$	2	0	1	0	1	2	1	2	0
$x_4=x_1+2x_2+1$	1	0	2	2	1	0	0	2	1

An eighteen trial plan was obtained by combining the two nine trial plans.
In order to estimate the effects of four parameters on each of the dust concentra-
tion coefficients for four feed size ranges specified in chapter 5, four feeds had to

98

be made. Thus, 72 experimental trials had to be carried out.

Experimental Procedure

Experimental preparation and operation were similar to those described in chapter 5. Coal particles and coal blocks were prepared from Waynesburg, Pittsburgh and Lower Kittanning coal seam, respectively. In running the experimental trials, coal blocks and coal particles were selected, rpm, the rate of feed and the depth of sump were set according to a given parametric combination, Four trials were run with ARCCS by feeding the same amount but different size of coal particles f_1, f_2, f_3, f_4 separately. In each trial, dust was sampled and the weights of collected dust on the sampler stages were measured. Then, another four trials were run under the next parametric combination.

Experimental Results and data

More than 216 dust samples had been taken in 72 trials. Because each trial lasted only 3 minutes, only the first three stages of the impactors collected dust in most of the experimental trials. In some trials, dust has been collected only on the first two stages of the impactors. Therefore, the total dust concentration of -15 microns, instead of dust size distributions, was analyzed. Furthermore, the bottom cascade impactor was often disturbed by falling coal particles. The data were not

reliable and were ignored. The data obtained from dust samples collected by the top and the middle cascade impactors are presented and analyzed as follows:

There were 72 dust samples collected by the top cascade impactor in 72 experimental trials. From each sample, a dust concentration coefficient was calculated for given feed particle size range and given parametric combination. Dust concentration coefficients obtained from 72 samples, for four particle size ranges and 18 parametric combinations, are listed in Table 6.7.

There were also 72 dust samples collected by the middle cascade impactor. Similarly, 72 dust concentration coefficients for the middle position with respect to cutting head were obtained as listed in Table 6.8.

Table 6.9 presents 72 average dust concentration coefficients obtained from the top and the middle cascade impactors. In the mathematical sense, the coefficients are denoted by $c_{dj}^{(i)}$, where i represents No. of combinations (i=1, 2, ..., 18) and j represents No. of feed particle size range (j=I, II, III and IV).

Table 6.7 Dust concentration coefficients
(from the top cascade impactors)

Combination		Dust concentration coefficients $(mg/m^3/kg)$			
		c_{d1}	c_{d2}	c_{d3}	c_{d4}
No.	Code	for range I	for range II	for range III	for range IV
1	0000	6.1	8.6	12.3	17.2
2	0112	9.4	16.8	18.3	30.4
3	0221	23.5	25.0	26.4	44.1
4	1011	14.0	18.4	23.5	29.4
5	1120	13.5	18.4	23.3	30.6
6	1202	17.3	27.8	28.8	30.4
7	2022	16.8	21.0	23.1	34.1
8	2101	13.2	21.3	28.6	35.2
9	2210	24.5	28.2	40.4	55.1
10	0021	10.3	15.4	20.6	25.0
11	0100	11.0	12.3	18.4	23.3
12	0212	13.1	18.9	22.0	32.0
13	1002	8.4	13.6	14.7	21.5
14	1111	18.4	19.1	26.4	32.3
15	1220	17.2	19.6	27.0	35.5
16	2010	9.8	17.2	20.8	23.3
17	2122	19.9	23.1	35.1	43.5
18	2201	24.2	28.6	33.8	54.3

Table 6.8 Dust concentration coefficients
(from middle cascade impactors)

No.	Code	c_{d1} for range I	c_{d2} for range II	c_{d3} for range III	c_{d4} for range IV
1	0000	12.3	15.9	18.4	23.3
2	0112	13.6	17.8	28.3	36.2
3	0221	23.5	26.4	30.1	47.7
4	1011	19.1	22.0	30.1	36.0
5	1120	20.8	25.7	28.2	38.0
6	1202	20.4	27.8	32.0	42.5
7	2022	20.4	23.1	29.4	36.2
8	2101	16.2	25.0	31.6	37.4
9	2210	29.4	34.3	49.0	61.3
10	0021	16.9	24.2	29.4	37.4
11	0100	18.4	20.8	23.3	27.0
12	0212	18.9	24.6	27.3	41.4
13	1002	14.7	17.8	22.0	32.0
14	1111	25.0	26.4	34.5	44.1
15	1220	25.7	29.4	44.1	49.0
16	2010	17.2	22.1	27.0	31.9
17	2122	29.4	40.4	46.1	53.5
18	2201	25.7	31.6	44.1	57.3

The header columns above span: Combination (No., Code) and Dust concentration coefficients ($mg/m^3/kg$).

Table 6.9 Dust concentration coefficients
(average of top and middle impactors)

| Combination | | Dust concentration coefficients $(mg/m^3/kg)$ | | | |
No.	Code	c_{d1} for range I	c_{d2} for range II	c_{d3} for range III	c_{d4} for range IV
1	0000	9.2	12.3	15.4	20.3
2	0112	11.5	17.3	23.3	33.3
3	0221	23.5	25.7	28.3	45.9
4	1011	16.6	20.2	26.8	32.7
5	1120	17.2	22.1	25.8	34.3
6	1202	18.9	27.8	30.4	36.5
7	2022	18.6	22.1	26.3	35.2
8	2101	14.7	23.2	29.9	36.3
9	2210	27.0	31.3	44.7	58.2
10	0021	13.6	19.8	25.0	31.2
11	0100	14.7	16.6	20.9	25.2
12	0212	16.0	21.8	24.7	36.7
13	1002	11.6	15.7	18.4	26.8
14	1111	21.7	22.8	30.5	38.2
15	1220	21.5	24.5	35.6	42.3
16	2010	13.5	19.7	23.9	27.6
17	2122	24.7	31.8	40.6	48.5
18	2201	25.0	30.1	39.0	55.8

Direct Estimation of the Effects

Utilizing the experimental data in Tables 6.9 and the direct estimation

method presented in Table 6.5, mean dust concentration coefficients at each level

with respect to each parameter and each feed particle size range were calculated as

shown in Tables 6.10.

Table 6.10 Direct estimation of the effects of factors
on dust concentration coefficients
(based on average of the top and middle impactors)

| Factor | Level | Mean dust concentration coefficients $(mg/m^3/kg)$ | | | |
| | | c_{d1} | c_{d2} | c_{d3} | c_{d4} |
		for range I	for range II	for range III	for range IV
x_1	0	14.8	18.9	22.9	32.1
	1	17.9	22.2	27.9	35.1
	2	20.6	26.3	34.0	43.6
x_2	0	13.8	18.3	22.6	28.9
	1	17.4	22.3	28.5	36.0
	2	22.0	26.9	33.8	45.9
x_3	0	15.7	20.9	25.6	33.5
	1	17.7	22.2	29.0	37.8
	2	19.8	24.3	30.2	39.6
x_3	0	17.2	21.0	27.7	34.6
	1	19.2	23.6	29.9	·40.0
	2	16.9	22.7	27.3	36.1

In the mathematical sense, data in Table 6.10 are denoted by $c_{dj}^{(b,k)}$, where k identify the parameters, for example, k=1 for x_1, and b represents code of level.

Based on the data presented in Tables 6.10, the effects of primary parameters on dust coefficients were directly evaluated as follows:

Particle Size

Dust concentration coefficient increases as feed particle size decreases. Dust concentration coefficient for particle size range IV (c_{d4}) is about two times as much as that for particle size range I (c_{d1}), as indicated in Tables 6.7-6.10. This is due to the fact that more particles and a greater total surface area are involved in a unit weight of smaller particles. Increasing the number of particles could increase the number of impact events and provide a larger total area of contact on the whole, hence generating more dust. This result reveals that a effective method to control the secondary dust generation is increasing the particle size in the product of the primary cutting. Since increasing depth of cut produces larger particles, it will help to reduce the amount of dust generated during the regrinding process.

Coal Properties x_1

All of dust concentration coefficients, c_{d1}, c_{d2}, c_{d3} and c_{d4}, vary with the type of coal, x_1. Lower Kittanning coal, represented by level 2, has the highest dust

concentration coefficient among the selected three types of coal, and Waynesburg

coal, represented by level 0, has the lowest as shown in Figures 6.1. Examining the

physical and mechanical properties of the coal seams, it was found that a relation-

ship exists between dust concentration coefficients and hardgrove grindability index

as shown in Figure 6.2. Dust concentration coefficients increase with increasing

hardgrove grindability index. This is because the material with a higher grindability

index results in more weight loss due to attrition. However, this may be true only

for the airborne dust level. For respirable dust levels, a hard material with a lower

grindability index may produce a larger amount of respirable dust than a soft

material because dust particles generated by hard materials have smaller sizes.
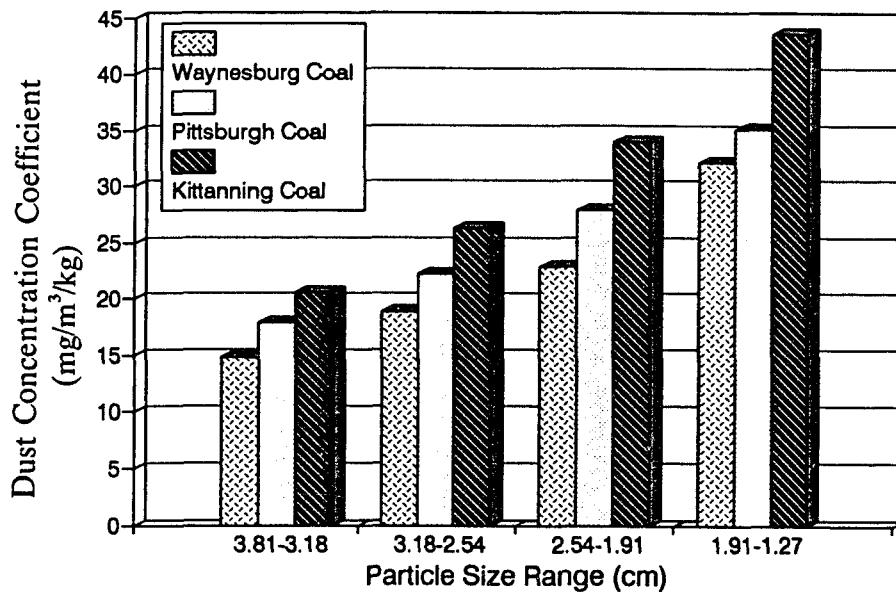
Figure 6.1. Effect of coal properties on dust concentration coefficients
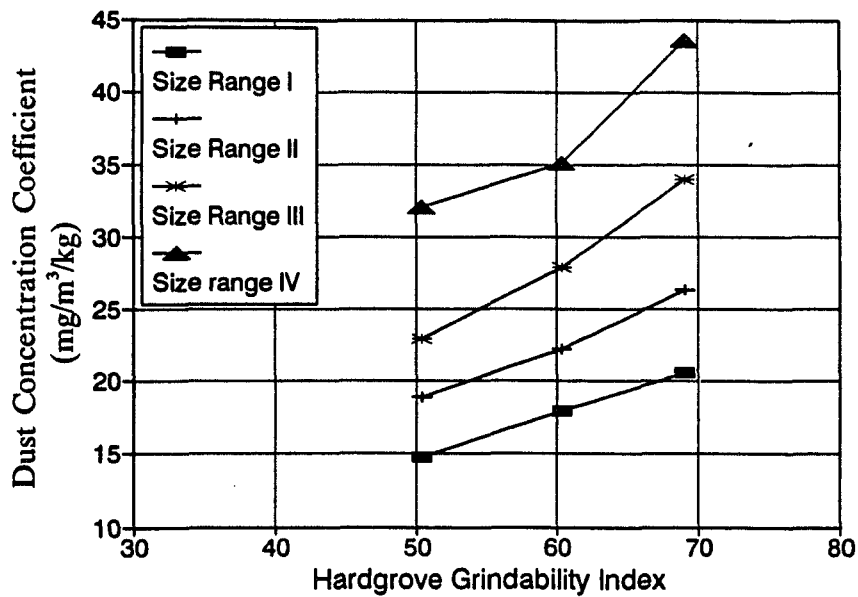
Figure 6.2. Relationship between dust concentration coefficients
and hardgrove grindability index

Depth of Sump x_2

Dust concentration coefficient for each size range increases with the depth of

sump, x_2, as shown in Figures 6.3. This is due to the fact that the length of cutting

path and the duration of regrinding are directly proportional to the depth of sump.

The deeper the sump, the more regrinding and more impact events could take

place. Therefore, reducing the depth of sump will effectively reduce the amount of

dust generated during the regrinding process.

107
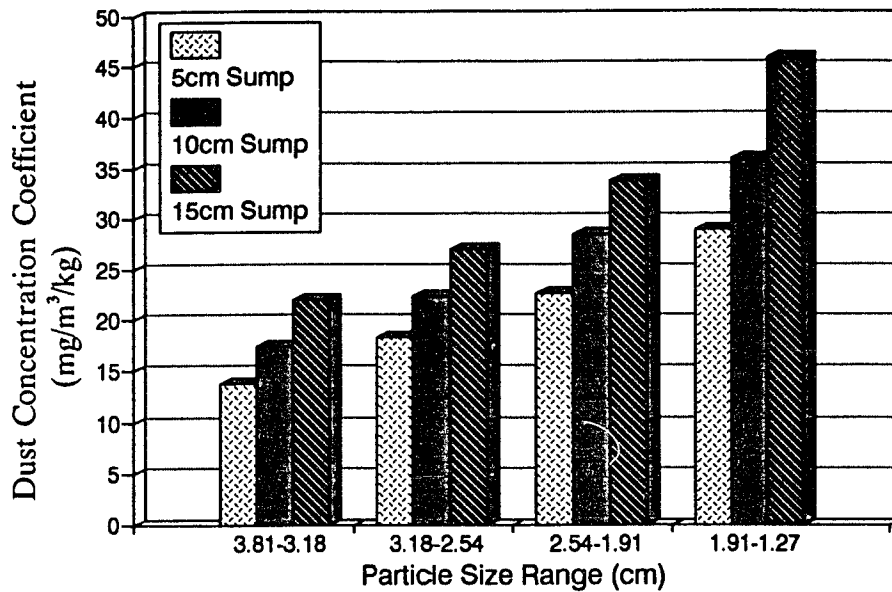
Figure 6.3. Effect of depth of sump on dust concentration coefficients

Cutting Velocity or rpm x_3

Dust concentration coefficient for each size range increases with the velocity of the cutting head, x_3. Theoretically, rpm is an important factor influencing impact failure. But the experimental results show that the effect of rpm is not as significant as that of the type of coal or the depth of sump, as indicated in Figures 6.4. This is due to the fact that rpm selected in the experiment was too low. All three levels of rpm were in the insignificant range. When the cutting head rotates at 45 rpm, the liner velocity of bit tip is about 1.14 m/s. This is much lower than the significant level suggested in the impact failure study presented in chapter 3. A

higher cutting velocity not only increases the secondary dust generation but also

cause the dust to become airborne. Therefore, deep and slow cutting not only

good for the primary cutting but also help to reduce the secondary dust generation.
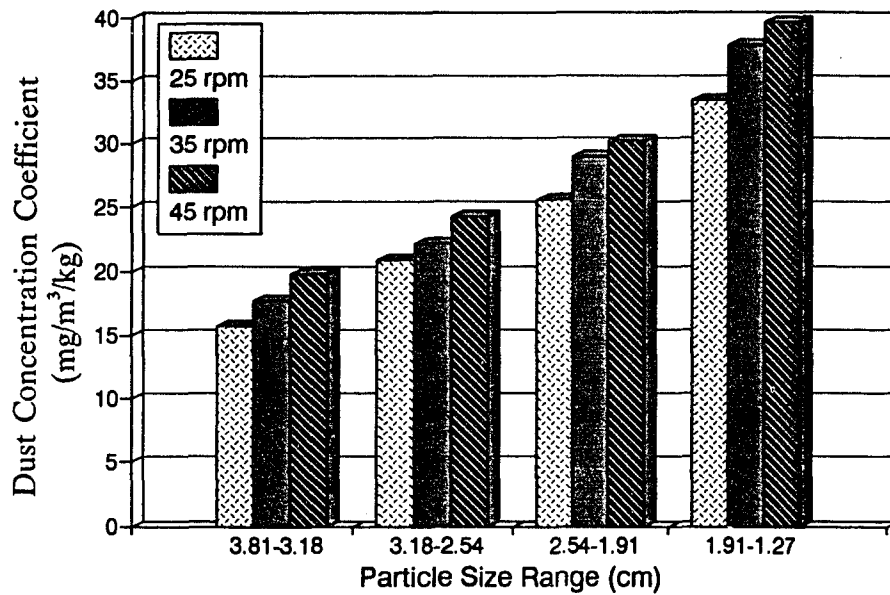
Figure 6.4. Effect of velocity of cutting head on dust concentration coefficients

Rate of Feed x_4

The results show that there is no correlations between dust concentration

coefficients and the rate of feed, x_4, as shown in Figures 6.5. This indicates that

dust generation by regrinding per unit weight of coal may not depend on the

amount of coal cut in each cutting cycle. However, total dust generation due to

regrinding is linearly proportional to the amount of total feed. If the coal is not loaded completely in each cutting cycle, The remainder coal will be subjected to regrinding. Therefore, it is important to load the coal as completely as possible in each cutting cycle to minimize the amount of coal subjected to regrinding.
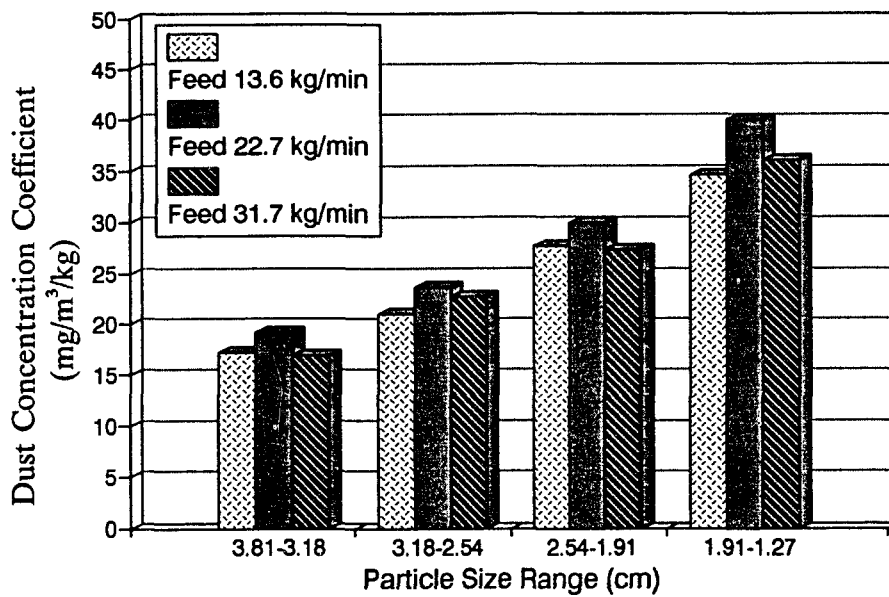
Figure 6.5. Effect of feed rate on dust concentration coefficients

Variance analysis

The effect of primary parameters on the secondary dust generation were also assessed by variance analysis. The experimental plan includes four parameters and three levels for each parameter. Each level of a parameter was repeated 6 times in

18 combinations. The variance, S, of dust concentration coefficients, c_{dj} (j=1, 2, 3 and 4), was calculated as follows.

Variability with respect to x_k is:

$$S_{x_k} - \frac{1}{6}\sum_{b-0}^{2}(6c_{dj}^{(b,k)})^2 - \frac{1}{18}(\sum_{i-1}^{18}c_{dj}^{(i)})^2 \tag{6.1}$$

where $c_{dj}^{(b,k)}$ is the mean dust concentration coefficients presented in Table 6.10 and $c_{dj}^{(i)}$ is the dust concentration coefficients presented in Table 6.9.

Total variability is:

$$S_t - \sum_{i-1}^{18}(c_{dj}^{(i)})^2 - \frac{1}{18}(\sum_{i-1}^{18}c_{dj}^{(i)})^2 \tag{6.2}$$

And the residual is:

$$S_e - S_t - \sum_{k-1}^{m}S_{x_k} \tag{6.3}$$

where m=4 is the number of factors.

Then, significance of each parameter was assessed based on variance analysis. Table 6.11 presents the method to assess the significance of each parameter by variance analysis.

111

Table 6.11 Significance assessment by variance analysis

Variabilities	Degree of freedom	Mean squares	Statistic Fx_k
Sx_k	2	$MSx_k=Sx_k/2$	MSx_k/MS_e
S_t	17		
S_e	9	$MS_e=S_e/9$	

Give significance level α. If $Fx_k > F_\alpha$ the factor is significant.
Otherwise, it is not significant.

Utilizing data presented in Tables 6.9-10, all variabilities were calculated and listed in Table 6.12. A statistical assessment of the effects of primary parameters on dust concentration coefficients for four feed side ranges has been made as shown in Table 6.13.

Variance analysis shows that the depth of sump has the most significant effect on dust concentration coefficients for all feed size ranges. Dust concentration coefficients for different types of coal are significantly different. The effect of cutting velocity on dust generation is not significant at $\alpha=0.05$ but it is significant at $\alpha=0.25$. As pointed out before, This is due to the fact that all three levels which were chosen in the experiment, are within insignificant range. The effect of the rate of feed is not significant.

Table 6.12 Variabilities of dust concentration coefficients
with respect to each factor for four feed size ranges

| Item | Variabilities of c_{dj} | | | |
	Range I	Range II	Range III	Range IV
S_t	457.7	498.1	1001.4	1735.1
Sx_1	101.4	166.5	373.8	427.1
Sx_2	198.6	220.1	372.7	869.5
Sx_3	52.1	35.2	68.0	118.2
Sx_4	18.9	20.5	23.8	92.8
S_e	86.7	54.8	163.0	227.4

Table 6.13 Assessment of the effects of parameters on dust
concentration coefficients by variance analysis

| Factor | on c_{d1} | | on c_{d2} | | on c_{d3} | | on c_{d4} | |
	Fx_k	Signif-icant	Fx_k	Signif-icant	Fx_k	Signifi-cant	Fx_k	Signif-icant
x_1	5.3	Yes	13.2	Yes	10.3	Yes	8.5	Yes
x_2	10.3	Yes	17.4	Yes	10.3	Yes	17.2	Yes
x_3	3.8	No	2.8	No	1.9	No	2.3	No
x_4	1.0	No	1.6	No	0.6	No	1.8	No

CONCLUSIONS

Coal particles, after being cut from a coal seam, are subjected to regrinding in the cutting path. Regrinding is a complicated size reduction process, where the mined coal particles are comminuted by three mechanisms, namely compression, impact, and attrition. A significant amount of coal dust is generated during the regrinding process.

Compression of coal particles produces coal dust because high stress concentration beneath the compressive force results in a crushed zone which yields fines and dust. The volume of the crushed zone and particle size of the crushed product depend on the degree of stress concentration and the properties of coal materials. A soft material yields a larger crushed zone than a hard material. However, the combination of hard materials and a higher stress concentration results in small sized dust and fine particles.

Impact of coal particles not only creates a crushed zone near the contact point, but also causes generated coal dust to become airborne. The volume of the crushed zone in impact failure and particle size of the crushed product depend on initial impact velocity and the properties of coal materials. A higher initial impact velocity results in a higher impact force and a larger crushed volume, generating a larger

114

amount of coal dust. The volume of the crushed zone is also linearly proportional to the initial impact velocity and increases with increasing Young's modulus of the material.

Attrition of coal particles generates a significant amount of airborne dust. This is because the size of fines and dust particles removed from the surface layer due to attrition is usually several microns and almost every coal particle, to a certain extent, is subjected to attrition. The amount of fines and dust generated due to attrition is directly proportional to the duration of regrinding and increases as feed particle size decreases.

Laboratory simulation of the regrinding process showed that only 5%~11% of the feed coal particles were subjected to compression or impact failure. The select function, the portion of the particles selected to break, is small and it decreases with feed particle size. But the amount of dust generated due to regrinding is significant and it increases as feed particle size decreases. The results indicate that attrition is the primary mechanism of the secondary dust generation. The significance of the secondary dust generation can be observed by the fact that regrinding 1 kg of coal particles in the coal cutting simulator produced 4~25 mg of airborne dust, depending on operating parameters and the properties of coal materials. It requires 2~12.5 m^3 air to dilute this amount of dust to an acceptable dust concentration level. In underground coal mines, if a face production is 2 tons/min and all mined coal is

subjected to regrinding, it may require 4000~25000 m^3 additional air to the face for diluting the dust or require other dust control techniques.

A factorial experimental study in the laboratory showed that dust generation by regrinding depends on the feed size distribution or on primary fragmentation. Small particles generated a larger amount of dust in the regrinding process than large particles. Dust concentration coefficients increased from 10~20 to 20~40 mg/m^3/kg when the size of feed particles decreased from 3.81 to 1.27 cm. This finding indicates that increasing the particle size in the product of the primary cutting is an effective method to control the secondary dust generation. It has been proven that deep cutting can reduce the primary dust generation and produce larger particles. Thus, deep cutting can also help to reduce dust generation during the regrinding process.

The depth of sump has the most significant effect on dust generation during regrinding. Laboratory experiments showed that the dust concentration coefficient, c_{d4}, increased form 28.9 to 45.9 mg/m^3/kg when the depth of sump increased from 5 to 15 cm. This result suggests that dust generation during regrinding could be effectively reduced by minimizing the distance of transit of coal particles through cutting path. This can be achieved by selecting proper depth of sump or altering sumping sequences.

Dust generation also significantly depends on the hardgrove grindability index of coal materials. For the airborne dust level, the coal with a higher grindability index has higher dust concentration coefficients. For the respirable dust level, more work

116

need to be done to evaluate the relationship. A higher velocity of cutting head causes, to a certain degree, a higher dust concentration. For example, the dust concentration coefficient, c_{d4}, increased from 33.5 to 39.6 mg/m^3/kg when rpm increased from 25 to 45.

Although dust concentration coefficients do not depend on the rate of feed, dust generated by regrinding is linearly proportional to the amount of feed. If the coal produced in each cutting cycle is not loaded completely, the remainder coal will be subjected to further regrinding. Therefore, loading the coal as completely as possible, in each cutting cycle, will help to reduce the effect of regrinding.

RECOMMENDATIONS FOR FURTHER RESEARCH

The depth of sump has the most significant effect on the amount of dust generated due to regrinding for a given particle size. The problem with deep sump is that the duration of regrinding increases with the depth of sump. Therefore reducing the depth of sump can limit regrinding of coal fragments. But simply reducing the depth of sump will reduce the productivity. The optimum depth of sump and sumping sequence should be studied.

The severity of the regrinding problem in coal cutting depends on the design of the cutting system. Compression, impact and attrition of coal particles in the cutting path vary greatly with bit spacing and the configuration of a cutting head. Regrinding in a continuous miner is significantly different from that in a longwall shearer. Linear cutting has a completely different configuration of cutting path from rotary cutting, hence having different regrinding situation. Studies of these subjects, in spite of being expensive, are strongly recommended.

This study investigated the significance of the secondary dust generation and the major affecting parameters for airborne dust levels. However for respirable dust levels, the experiments did not provide sufficient data for the similar analysis. As indicated in

the appendix, some of dust samplers collected dust only on the stages which have a GMD (Geometric Mean Diameter) greater than 5 microns. More experiments need to be carried out in order to obtain a complete dust size distribution and to analyze dust generation for different dust size levels.

To control overall dust generation, another area to be investigated is the quantitative comparison of the secondary dust generation with the primary dust generation.

REFERENCES

Angel, P. A., 1976, *Impact Wear of Materials*, Elsevier Scientific Publishing Company, New York.

Arbiter, N., Harris, C. C. and Stambolizis, G. A., 1969, "Single Fracture of Brittle Spheres," *Trans. SME/AIME, 244*, 118-133.

Bond, F. C., 1952, "The Third Theory of Comminution," *Min. Eng. Trans. AIME, 193*, 484-494.

Broadbent, S. R. and Callcott, T. G., 1956a, "A Matrix Analysis of Processes Involving Particle Assemblies'" *Phil. Trans. R. Soc., 249*, 99-123.

Broadbent, S. R. and Callcott, T. G., 1956b, "A New Analysis of Coal Breakage Process," *J. Inst. Fuel, 29*, 524-528.

Daniel, J. H., 1984, "Respirable Dust Control Research--The Bureau of Mines Program," *Proc. of 1984 Coal Mine Dust Conference*, West Virginia University, 1-8.

Dey, A., 1985, "Orthogonal Resolution III Designs for Symmetrical and Asymmetrical Factorials," *Orthogonal Fractional Factorial Design*, Wiley, New York, pp. 24-73.

Hamilton M. and Goodman, E., 1966, "The Stress Field Created by a Circular Sliding Contact," *J. App. Mech., 33*, 371-376.

Jaeger, J. C., 1967, "Failure of Rocks Under Tensile Conditions," *Int. J. Rock Mech. Miner. Sci.*, 4, 291-237.

Johnson, W., 1972, *Impact Strength of Materials*, London Edward Arnold.

Khair, A. W., 1984, "Study of Fracture Mechanisms in Coal Subjected to Various Types of Surface Traction Using Holographic Interferometry," *Proc. of 25th U.S. Symp. on Rock Mechanics*, 103-114.

Khair, A. W. and Reddy, N. P., 1985, "The Effect of In-situ and Operating Parameters on Fragmentation of Coal," *Supplemented with Proc. of 26th U.S. Symp. on Rock Mechanics*, June 26-28.

Khair, A. W., 1984, "Design and Fabrication of a Rotary Coal Cutting Simulator," *Proc. of 1984 Coal Mine Dust Conference*, West Virginia University, 190-197.

Khair, A. W. and Xu, D., 1990, "Mechanism of Regrinding in Rotary Cutting Machines," *Proc. of Symp. on Respirable Dust in The Mineral Industries*, October 17-19.

Lowrison, G. C., 1974, "Impact Machines," *Crushing and Grinding*, CRC Press, Inc. Cleveland, Ohio, 191-223.

Lynch, A. J., 1977, "Fundamentals of Comminution & Mathematical Models of Size-Reduction Processes," *Mineral Crushing and Grinding Circuits*, Elsevier North-Holland, New York, pp. 1-44.

Prasher, C. L., 1987, *Crushing and Grinding Process Handbook*, John Wiley & Sons

Limited, New York.

Roepke, W. W., 1984, "General Methods of Primary Dust Control During Cutting,"
Min. Eng., June, Vol.36, 636-644.

Rineheart, J. S., 1960, "The Role of Stress Waves in the Comminution of Brittle
Rocklike Materials," *Int. Symp. on Stress Wave Propagation*, Interscience
Publishing Inc., New York, 247-269.

Rosin, P. and Rammler, E., 1933, "The Laws Governing the Fineness of Pulverized
Coal," *J. Inst. Fuel*, 7, 29-36.

Timoshenko, K., and Goodier, J. N., 1951, *Theory of Elasticity*, McGraw-Hill Book Co.
New York.

Voltz, J. I., 1989, "Effect of Energy and Impact Direction on Coal Fragmentation,"
RI 9260, USBM.

Zukas, J. A., 1982, "Damage in Composite Material Due to Low Velocity Impact,"
Impact Dynamics, Wiley, New York, pp. 55-94.

APPENDIX

EXPERIMENTAL DATA

Table A.1 Data from the top cascade impactors

Combination		Feed size range	The amount of dust (mg)					
No.	Code		Stage 3	Stage 4	Stage 5	Stage 6	Stage 7	Total
1	0000	I	0.4	0.1				0.5
		II	0.5	0.1	0.1			0.7
		III	0.7	0.2	0.1			1.0
		IV	0.9	0.3	0.2			1.4
2	0112	I	1.5	0.2	0.1			1.8
		II	2.5	0.5	0.2			3.2
		III	2.3	0.8	0.3	0.1		3.5
		IV	4.1	1.0	0.6	0.1		5.8
3	0221	I	2.2	0.8	0.2			3.2
		II	2.3	0.7	0.3	0.1		3.4
		III	2.6	0.6	0.3	0.1		3.6
		IV	4.0	1.2	0.7	0.1		6.0

A 296 cascade impactor consists of six stages, stage 3 to stage 8, and a backup filter. Stage 3 has a Geometric Mean Diameter (GMD) of 12.25 microns. Stage 4 has a GMD of 7.75 microns. Stage 5 has a GMD of 4.58 microns. Stage 6 has a GMD of 2.65 microns. Stage 7 has a GMD of 1.34 microns. Combination No. and Code are referred to Tables 6.5-6. Feed size ranges are given in chapter 5.

Table A.1 (cont'd)

| Combination | | Feed size range | The amount of dust (mg) | | | | | |
No.	Code		Stage 3	Stage 4	Stage 5	Stage 6	Stage 7	Total
4	1011	I	1.4	0.4	0.1			1.9
		II	1.7	0.6	0.2			2.5
		III	2.2	0.7	0.3			3.2
		IV	2.7	0.9	0.4			4.0
5	1120	I	0.8	0.2	0.1			1.1
		II	1.1	0.3	0.1			1.5
		III	1.3	0.4	0.2			1.9
		IV	1.6	0.5	0.3	0.1		2.5
6	1202	I	2.1	0.9	0.2	0.1		3.3
		II	2.9	1.5	0.6	0.2	0.1	5.3
		III	3.6	1.1	0.5	0.2	0.1	5.5
		IV	4.1	1.0	0.4	0.2	0.1	5.8
7	2022	I	2.3	0.5	0.3	0.1		3.2
		II	3.1	0.5	0.3	0.1		4.0
		III	3.4	3.6	0.3	0.1		4.4
		IV	5.0	1.1	0.3	0.1		6.5
8	2101	I	1.4	0.3	0.1			1.8
		II	2.0	0.5	0.3	0.1		2.9
		III	2.5	0.8	0.5	0.1		3.9
		IV	2.9	1.2	0.6	0.1		4.8

Combination		Feed size range	The amount of dust (mg)					
No.	Code		Stage 3	Stage 4	Stage 5	Stage 6	Stage 7	Total
9	2210	I	1.2	0.5	0.2	0.1		2.0
		II	1.6	0.4	0.2	0.1		2.3
		III	2.2	0.6	0.4	0.1		3.3
		IV	3.5	0.7	0.2	0.1		4.5
10	0021	I	0.9	0.3	0.2			1.4
		II	1.6	0.3	0.1	0.1		2.1
		III	1.9	0.5	0.3	0.1		2.8
		IV	2.1	0.8	0.4	0.1		3.4
11	0100	I	0.7	0.1	0.1			0.9
		II	0.7	0.2	0.1			1.0
		III	1.0	0.3	0.2			1.5
		IV	1.5	0.3	0.1			1.9
12	0212	I	1.9	0.4	0.2			2.5
		II	2.5	0.7	0.3	0.1		3.6
		III	2.9	0.9	0.3	0.1		4.2
		IV	4.3	1.1	0.6	0.1		6.1
13	1002	I	1.1	0.3	0.2			1.6
		II	2.0	0.4	0.2			2.6
		III	2.1	0.5	0.2			2.8
		IV	2.9	0.8	0.4			4.1

Table A.1 (cont'd)

Combination		Feed size range	The amount of dust (mg)					
No.	Code		Stage 3	Stage 4	Stage 5	Stage 6	Stage 7	Total
14	1111	I	1.7	0.4	0.3	0.1		2.5
		II	1.7	0.6	0.2	0.1		2.6
		III	2.4	0.8	0.3	0.1		3.6
		IV	2.7	1.0	0.5	0.2		4.4
15	1220	I	0.8	0.3	0.2	0.1		1.4
		II	1.0	0.3	0.2	0.1		1.6
		III	1.5	0.4	0.2	0.1		2.2
		IV	1.9	0.7	0.2	0.1		2.9
16	2010	I	0.4	0.2	0.1	0.1		0.8
		II	1.0	0.2	0.1	0.1		1.4
		III	1.1	0.3	0.2	0.1		1.7
		IV	1.2	0.4	0.2	0.1		1.9
17	2122	I	2.8	0.7	0.2	0.1		3.8
		II	2.8	1.1	0.3	0.1		4.4
		III	4.6	1.5	0.5	0.1		6.7
		IV	5.7	1.8	0.7	0.1		8.3
18	2201	I	2.3	0.5	0.4	0.1		3.3
		II	2.8	0.6	0.4	0.1		3.9
		III	3.5	0.7	0.3	0.1		4.6
		IV	5.3	1.4	0.6	0.1		7.4

127

Table A.2 Data from the middle cascade impactors

| Combination | | Feed size range | The amount of dust (mg) | | | | | |
No.	Code		Stage 3	Stage 4	Stage 5	Stage 6	Stage 7	Total
1	0000	I	0.8	0.2				1.0
		II	1.0	0.2	0.1			1.3
		III	1.1	0.3	0.1			1.5
		IV	1.2	0.5	0.2			1.9
2	0112	I	2.0	0.5	0.1			2.6
		II	2.6	0.6	0.2			3.4
		III	4.0	0.9	0.4	0.1		5.4
		IV	5.0	1.2	0.6	0.1		6.9
3	0221	I	2.5	0.5	0.2			3.2
		II	2.6	0.6	0.3	0.1		3.6
		III	3.0	0.7	0.3	0.1		4.1
		IV	4.0	1.8	0.6	0.1		6.5

A 296 cascade impactor consists of six stages, stage 3 to stage 8, and a backup filter. Stage 3 has a Geometric Mean Diameter (GMD) of 12.25 microns. Stage 4 has a GMD of 7.75 microns. Stage 5 has a GMD of 4.58 microns. Stage 6 has a GMD of 2.65 microns. Stage 7 has a GMD of 1.34 microns. Combination No. and Code are referred to Tables 6.5-6. Feed size ranges are given in chapter 5.

Table A.2 (cont'd)

Combination		Feed size range	The amount of dust (mg)					
No.	Code		Stage 3	Stage 4	Stage 5	Stage 6	Stage 7	Total
4	1011	I	1.5	0.6	0.4	0.1		2.6
		II	1.8	0.7	0.4	0.1		3.0
		III	2.6	0.8	0.6	0.1		4.1
		IV	3.2	1.0	0.6	0.1		4.9
5	1120	I	1.3	0.3	0.1			1.7
		II	1.6	0.4	0.1			2.1
		III	1.7	0.4	0.2			2.3
		IV	2.0	0.7	0.3	0.1		3.1
6	1202	I	2.6	0.8	0.4	0.1		3.9
		II	3.5	1.1	0.4	0.2	0.1	5.3
		III	3.9	1.3	0.6	0.2	0.1	6.1
		IV	5.6	1.5	0.7	0.2	0.1	8.1
7	2022	I	3.0	0.5	0.3	0.1		3.9
		II	3.3	0.6	0.4	0.1		4.4
		III	4.1	0.8	0.6	0.1		5.6
		IV	5.0	1.3	0.5	0.1		6.9
8	2101	I	1.5	0.4	0.2	0.1		2.2
		II	2.5	0.5	0.3	0.1		3.4
		III	2.9	0.8	0.5	0.1		4.3
		IV	3.7	1.1	0.3	0.1		5.1

129

Combination		Feed size range	The amount of dust (mg)					
No.	Code		Stage 3	Stage 4	Stage 5	Stage 6	Stage 7	Total
9	2210	I	1.6	0.5	0.2	0.1		2.4
		II	2.1	0.4	0.2	0.1		2.8
		III	2.7	0.7	0.5	0.1		4.0
		IV	3.6	0.8	0.5	0.1		5.0
10	0021	I	1.8	0.4	0.1			2.3
		II	2.3	0.7	0.2	0.1		3.3
		III	2.7	0.8	0.4	0.1		4.0
		IV	2.9	1.5	0.6	0.1		5.1
11	0100	I	1.2	0.2	0.1			1.5
		II	1.3	0.3	0.1			1.7
		III	1.3	0.4	0.2			1.9
		IV	1.5	0.5	0.2			2.2
12	0212	I	3.0	0.5	0.1			3.6
		II	3.5	0.8	0.4			4.7
		III	4.0	0.9	0.3			5.2
		IV	5.1	2.1	0.6	0.1		7.9
13	1002	I	2.3	0.3	0.2			2.8
		II	3.0	0.3	0.1			3.4
		III	2.9	0.8	0.5			4.2
		IV	4.5	0.9	0.6	0.1		6.1

Table A.2 (cont'd)
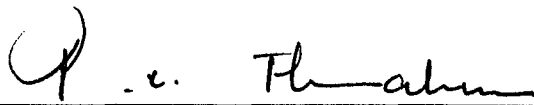
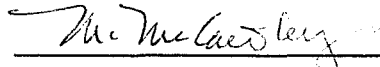| Combination		Feed size range	The amount of dust (mg)					
No.	Code		Stage 3	Stage 4	Stage 5	Stage 6	Stage 7	Total
14	1111	I	2.7	0.5	0.2			3.4
		II	2.8	0.5	0.3			3.6
		III	3.3	0.9	0.5			4.7
		IV	4.3	1.1	0.5	0.1		6.0
15	1220	I	1.4	0.4	0.2	0.1		2.1
		II	1.6	0.5	0.2	0.1		2.4
		III	2.3	0.8	0.4	0.1		3.6
		IV	2.6	0.9	0.4	0.1		4.0
16	2010	I	0.8	0.3	0.2	0.1		1.4
		II	1.2	0.3	0.2	0.1		1.8
		III	1.5	0.4	0.2	0.1		2.2
		IV	1.8	0.5	0.3			2.6
17	2122	I	4.2	1.1	0.2	0.1		5.6
		II	4.9	2.0	0.7	0.1		7.7
		III	4.9	2.7	1.1	0.1		8.8
		IV	6.4	2.6	1.1	0.1		10.2
18	2201	I	2.6	0.6	0.2	0.1		3.5
		II	3.2	0.7	0.3	0.1		4.3
		III	4.7	0.7	0.5	0.1		6.0
		IV	5.3	1.7	0.6	0.2		7.8

VITA

Danqing Xu was born in Fujian, the People's Republic of China, on March 28, 1960. He began his college career at Fuzhow University in October, 1978 and received a B.S. in mining engineering in July, 1982. Then he attended Beijing Graduate School of China University of Mining and Technology and graduated with a M.S. in mining engineering in July, 1985. He was employed in Beijing Graduate School of China University of Mining and Technology from August, 1982 to November, 1987.

He entered West Virginia University in January, 1988. Since then he has been a graduate assistant in the Department of Mining Engineering at West Virginia University working toward his doctoral degree.
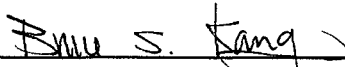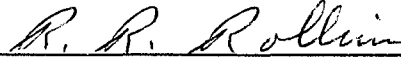
APPROVAL OF EXAMINING COMMITTEE
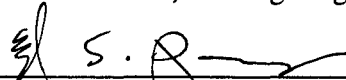
P. C. Thakur, CONSOL INC.
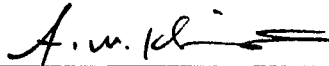
M. McCawley, NIOSH

S. Bruce Kang, Mechanical Engineering

R. R. Rollins, Mining Engineering

Syd. S. Peng, Mining Engineering

7/31/92

Date

A. W. Khair, Mining Engineering
Chairman of Committee